

RESEARCH ARTICLE

Neuronal NADPH oxidase 2 regulates growth cone guidance downstream of slit2/robo2

Aslihan Terzi ^{1,2} | Haley Roeder^{1,2} | Cory J. Weaver^{1,2} | Daniel M. Suter ^{1,2,3,4}

¹Department of Biological Sciences, Purdue University, West Lafayette, IN, USA

²Purdue Institute for Integrative Neuroscience, Purdue University, West Lafayette, IN, USA

³Bindley Bioscience Center, Purdue University, West Lafayette, IN, USA

⁴Birck Nanotechnology Center, Purdue University, West Lafayette, IN, USA

Correspondence

Daniel M. Suter, Department of Biological Sciences, Purdue University, 915 West State Street, West Lafayette, IN 47907-2054, USA.

Email: dsuter@purdue.edu

Present address

Cory J. Weaver, Department of Biological Sciences, University of South Carolina, Columbia, SC, USA

Funding information

Office of the Executive Vice President for Research and Partnerships at Purdue University, Grant/Award Number: 210362; Division of Integrative Organismal Systems, Grant/Award Number: 1146944-IOS; Purdue Research Foundation, Grant/Award Number: 209911; Indiana Traumatic Spinal Cord and Brain Injury Research Fund, Grant/Award Number: 20000289; National Institute of Neurological Disorders and Stroke, Grant/Award Number: R01NS117701

Abstract

NADPH oxidases (Nox) are membrane-bound multi-subunit protein complexes producing reactive oxygen species (ROS) that regulate many cellular processes. Emerging evidence suggests that Nox-derived ROS also control neuronal development and axonal outgrowth. However, whether Nox act downstream of receptors for axonal growth and guidance cues is presently unknown. To answer this question, we cultured retinal ganglion cells (RGCs) derived from zebrafish embryos and exposed these neurons to netrin-1, slit2, and brain-derived neurotrophic factor (BDNF). To test the role of Nox in cue-mediated growth and guidance, we either pharmacologically inhibited Nox or investigated neurons from mutant fish that are deficient in Nox2. We found that slit2-mediated growth cone collapse, and axonal retraction were eliminated by Nox inhibition. Though we did not see an effect of either BDNF or netrin-1 on growth rates, growth in the presence of netrin-1 was reduced by Nox inhibition. Furthermore, attractive and repulsive growth cone turning in response to gradients of BDNF, netrin-1, and slit2, respectively, were eliminated when Nox was inhibited in vitro. ROS biosensor imaging showed that slit2 treatment increased growth cone hydrogen peroxide levels via mechanisms involving Nox2 activation. We also investigated the possible relationship between Nox2 and slit2/Robo2 signaling in vivo. *astray/nox2* double heterozygote larvae exhibited decreased area of tectal innervation as compared to individual heterozygotes, suggesting both Nox2 and Robo2 are required for establishment of retinotectal connections. Our results provide evidence that Nox2 acts downstream of slit2/Robo2 by mediating growth and guidance of developing zebrafish RGC neurons.

KEYWORDS

axon growth and guidance, hydrogen peroxide, NADPH oxidase, optic chiasm, optic tectum, reactive oxygen species, retinal ganglion cell, Robo2, slit2

1 | INTRODUCTION

Reactive oxygen species (ROS) are now well accepted as second messengers in cellular signaling events in many different cell types and processes, including stem cell maintenance, cell differentiation, and migration (Chaudhari

et al., 2014; Finkel, 2011; Reczek & Chandel, 2015; Wang et al., 2013). ROS also control central nervous system development and function (Acker & Acker, 2004; Bórquez et al., 2016; Halliwell, 1992; Safiulina et al., 2006). Recent work by several groups including ours suggests a role for ROS signaling in neuronal development, specifically in neuronal progenitor cell proliferation and differentiation (Dickinson et al., 2011; Suzukawa et al., 2000), cerebellar

Aslihan Terzi and Haley Roeder should be considered joint first author.

development (Coyoy et al., 2013; Olguín-Albuérne & Morán, 2015), axonal growth, neuronal polarity, and growth cone motility (Morinaka et al., 2011; Munnamalai et al., 2014; Munnamalai & Suter, 2009; Wilson et al., 2015), and the formation of retinotectal connections (Gauron et al., 2016; Weaver et al., 2018). A key source of cellular ROS is nicotinamide adenine dinucleotide phosphate (NADPH) oxidases (NOX), which are a class of membrane-bound multimeric enzyme complexes that catalyze the reduction of molecular oxygen to superoxide (Babior, 2004; Bedard & Krause, 2007). There are seven known NOX isoforms in humans, NOX1-5, Dual Oxidase (DUOX) 1 and DUOX2, which have distinct cell type-specific expression patterns and functions (Bedard & Krause, 2007; Brandes & Kreuzer, 2005; Nayernia et al., 2014). We have recently reviewed the role of NOX-derived ROS in neuronal development in detail (Terzi & Suter, 2020).

NOX2 is the first NOX isoform to be identified originally in phagocytes and is best understood with respect to expression, regulation, and function (Nauseef, 2004). The functional NOX2 complex consists of catalytic transmembrane subunit and cytosolic subunits for activation. NOX2 is expressed by neurons (Cao et al., 2009; Hilburger et al., 2005; Munnamalai et al., 2014; Tejada-Simon et al., 2005; Wilson et al., 2015), astrocytes (Lin et al., 2012), and microglia (Cooney et al., 2014). Nox2 and the cytosolic subunit p40phox are closely associated with F-actin at the growth cone periphery, and Nox inhibition reduces actin content and dynamics, as well as growth cone motility and neurite outgrowth in *Aplysia* bag cell neurons (Munnamalai et al., 2014; Munnamalai & Suter, 2009). Furthermore, local clustering of the *Aplysia* cell adhesion molecule apCAM increases co-localization of Nox2 with p40phox and neurite growth (Munnamalai et al., 2014), indicating that Nox2 signaling downstream of apCAM could regulate neurite growth.

The establishment of retinotectal connections between retinal ganglion cells (RGCs) and the optic tectum (OT) is a frequently investigated model system for axonal pathfinding and has been well characterized in embryonic zebrafish (Kita et al., 2015; Poulain et al., 2010; Stuermer, 1988). RGCs are the first cell type in the retina to differentiate from neural progenitor cells beginning around 28 hour (h) postfertilization (hpf) (Hu & Easter, 1999). These cells send their axons toward the optic disk, where they fasciculate and exit the eye as the optic nerve (ON). From there, the axons extend toward the brain, form the optic chiasm (OC), cross to the contralateral side, and ultimately, find their synaptic targets in the OT. To establish this highly stereotypic connection, RGC axons must make multiple guidance decisions along their route based on topographic and molecular cues in their environment. First, nascent RGCs send axons medially toward the optic disk, where surrounding neuroepithelial cells secrete netrin-1, which attracts retinal axons toward the disk

(De La Torre et al., 1997; Deiner et al., 1997). After exiting the eye, the RGC axons fasciculate to form the ON. The cells surrounding the ON secrete slit2 to prevent aberrant ON projections and to form the chiasm at the proper location (Erskine et al., 2000; Fricke et al., 2001; Plachez et al., 2008; Thompson et al., 2006). Furthermore, brain-derived neurotrophic factor (BDNF) decreases dendritic arborization in the retina, while increasing axonal arborization in the tectum (Lom & Cohen-Cory, 1999). Zebrafish embryos exhibit relative broad expression of Nox1, Nox2, Nox5, and Duox in the central nervous system, including in the eyes and the brain during the first 48 hpf (Weaver et al., 2016). We have recently found, in vivo, that pharmacological Nox inhibition, as well as Nox2 deficiency, severely affects the formation of the ganglion cell layer in the retina and the formation of connections between the RGCs and the developing zebrafish brain (Weaver et al., 2018). A role for H₂O₂ in zebrafish retinotectal pathfinding was also proposed by another group (Gauron et al., 2016). Altogether, these results suggest that Nox2-derived ROS may be involved in downstream signaling of specific axonal growth and guidance receptors. However, the molecular details of upstream activation by guidance receptors and downstream effectors of ROS signaling in axonal growth and guidance in a cell-autonomous manner have not been demonstrated thus far.

Here, we show that slit2-mediated axonal growth and guidance of cultured zebrafish RGC neurons depends on Nox activation, specifically on Nox2. Furthermore, we show that the growth cone guidance effects of netrin-1 and BDNF are also regulated by Nox activity. We also demonstrate that slit2/Robo2 and Nox2 activation are both required for RGCs to properly make projections in the OT in vivo. In conclusion, we provide the first evidence that chemotropic growth cone guidance responses depend on Nox2 activity in a cell-autonomous manner, most likely via H₂O₂ as second messengers.

2 | MATERIALS AND METHODS

2.1 | Zebrafish housing/breeding

All animal experiments were ethically reviewed and approved by the Purdue Animal Care and Use Committee (PACUC), following NIH guidelines with the protocol 1201000592 approved on 04/09/2017. Zebrafish (*Danio rerio*) of the AB, *Tg(ath5:GFP)*, *nox2*^{-/-}, *astray*[±] lines were maintained according to standard procedures (Hensley & Leung, 2010; Westerfield, 2000). Parental fish were set in pairs and embryos were collected 15 minute (min) after breeding to obtain cohorts of the same stage. Embryos were maintained in E3 medium (i.e., 5 mM NaCl, 0.17 mM KCl, 0.33 mM CaCl₂, 0.33 mM MgSO₄, and 10⁻⁵% Methylene Blue) at 28°C and staged prior to harvest (Kimmel et al., 1995).

2.2 | Mutant fish lines

We created *nox2*^{-/-} mutant fish lines using the clustered regularly interspaced short palindromic repeats (CRISPR)/Cas9 genome editing technique. We used two different guide RNAs that target the N-terminal region of Nox2, both resulting in truncated nonfunctional Nox2 enzymes. Guide RNA I results in a 33 amino acid peptide, whereas guide RNA II results in a 221 amino acid peptide, lacking substrate binding and enzymatic domains. These Nox2-deficient fish lines were created in both AB and *Tg(ath5:GFP)* background and confirmed by genotyping and sequencing. The details of these lines have been previously described (Weaver et al., 2018). Unless otherwise is stated, we used *nox2*^{pu22} (ZFIN Cat# ZDB-GENO-190822-7, RRID:ZFIN_ZDB-GENO-190822-7) mutants that were generated from guide RNA I throughout this article. Astray has been identified as *robo2*-deficient mutant in zebrafish. The *astray*^{ti272z} mutants were previously characterized by Fricke et al. (2001) and kindly provided to us by the lab of Dr. Michael Granato (University of Pennsylvania).

2.3 | Genotyping

Genomic DNA was isolated from 24 to 96 hpf tail biopsies (Wilkinson et al., 2013). Samples were dissolved in 50 mM of NaOH by incubating for 10 min at 95°C. DNA samples were neutralized with 1 M of Tris HCl pH 8.0 and stored at -20°C until further processing. The *nox2*^{-/-} mutants were genotyped with the DNA polyacrylamide gel method described by Zhu et al. (2014). Following PCR amplification with GoTaq Flexi (Promega, Cat#M8291, Madison, WI), samples were heated to 95°C and allowed to cool for 10 min at room temperature (RT). Samples were then loaded onto a 15% of acrylamide gel without SDS and run for 2.5 h at 150 V. Gels were stained with GelRed Nucleic Acid stain (Biotium, Cat#41003, Fremont, CA) for 10 min to visualize DNA bands. Heteroduplexes indicative of heterozygous mutants exhibited lower electrophoretic mobility compared to homoduplexes indicative of wildtype or homozygous mutants, which can be further differentiated by their size differences (Zhu et al., 2014). *Astray*[±] and *astray*^{-/-} mutants were genotyped using site-specific primers to differentiate wildtype and mutant alleles (Kastenhuber et al., 2009). After PCR amplification, samples were loaded onto a 2% of agarose gel. Presence of amplification from both wildtype and mutant primers indicated heterozygosity. Following primers were used for genotyping: *nox2* (F): 5'-CCCAGATAGCTTACGATAACAAA-3'; *nox2* (R): 5'-CTCTCGATCTCATCTCCTGAT-3'; *astray* (F): 5'-GAATGACTCCTCGTCGCTCT-3'; *astray* wildtype

allele (R): 5'-CAGCTCCTTTTGCACATGTTT-3'; *astray* mutant allele (R): 5'-CAGCTCCTTTTGCACATGTTA-3'.

2.4 | Dissociated RGC neuronal culture

The protocol was modified from a previous study (Chen et al., 2013). At 33–34 hpf embryos were sterilized with 70% of ethanol and transferred to a new dish containing E2 medium (i.e., 15 mM NaCl, 0.5 mM KCl, 1 mM MgSO₄, 0.15 mM KH₂PO₄, 0.05 mM Na₂HPO₄, 1.0 mM CaCl₂, and 0.7 mM NaHCO₃). Chorions were removed with sharp forceps, and embryos were sacrificed by decapitation. Whole eyes were extracted, triturated 30 times in L15 medium (Invitrogen, Carlsbad, CA) supplemented with 2% of FBS (Thermo Scientific, Waltham, MA), 0.4% of pen/strep, and 12.5% of saline solution (10 mM D-glucose, 5 mM Na-pyruvate, 1.26 mM CaCl₂, and 32 mM HEPES) using a P20 pipette. Individual cells were then plated on coverslips pre-coated with 0.5 mg/ml of poly-D-lysine (70–150 kD) (Sigma, St. Louis, MO) for 20 min, washed with PBS, and then, coated with 20 µg/ml of laminin (Invitrogen, Carlsbad, CA) for 6 h. Cells were maintained in supplemented L15 medium in 35 mm petri dishes overnight at RT.

2.5 | Axonal growth assay with cultured RGCs

For live-cell imaging, coverslips containing overnight retinal cultures were transferred from culture dishes to a custom-made open imaging chamber described previously (Suter, 2011). Prior to imaging, medium was replaced with serum-free L15 medium without phenol red. Imaging was performed with a Nikon TE2000 Eclipse microscope (Nikon, Melville, NY), a 60× 1.4 NA oil differential interference contrast (DIC) objective with additional 1.5× magnification (90× total), a OG590 long-pass red filter (Chroma Technology Corp., Bellows Falls, VT) and a Cascade II cooled EM-CCD camera (Photometrics, Tucson, AZ). RGCs were identified by positive GFP fluorescence, and initial DIC images of isolated neurons were acquired at time = 0 min. After imaging, medium was replaced with L15 containing 0.1% of DMSO (vehicle control), different cues (slit2 (10 µg/ml); netrin-1 (0.1 µg/ml); and BDNF (0.01 µg/ml; R&D Systems, Inc., Minneapolis, MN)), or pan-Nox inhibitors Celastrol (CST; 0.05 µM; Cayman Chemical, Ann Arbor, MI) or VAS2870 (0.5 µM; Enzo Life Sciences, Farmingdale, NY). Additional images were acquired at 15 and 30 min. Using MetaMorph 7.8 software (MetaMorph Microscopy Automation and Image Analysis Software, RRID:SCR_002368; Molecular Devices, Sunnyvale, CA), axonal lengths were measured from the base of the cell body to the tip of the growth cone

lamellipodia on neurons with processes $\geq 15 \mu\text{m}$. Axonal growth rates of individual RGCs were determined by subtracting the initial length from final length and dividing the growth difference by the elapsed time. Percent growth cone collapse was determined by counting the number of growth cones that are collapsed in response to cue treatment per experiment. Bullet shaped axonal tips, occasionally with a single filopodium and/or lacking lamellipodia were considered as collapsed growth cones. Growth cones harboring a flattened filopodia and/or with ≥ 2 filopodia were not considered as collapsed growth cones.

2.6 | Guidance assay with cultured RGCs

Micropipettes were pulled from borosilicate glass capillaries (1B100F-4; World Precision Instruments, Sarasota, FL) with a Narishige pipette puller (PP-830, Narishige, Amityville, NY) to produce an average inner tip diameter of $1.0 \mu\text{m}$. Micropipettes with internal diameters of $1.0\text{--}1.5 \mu\text{m}$ were used for guidance experiments. Gradients were generated according a previously reported method (Lohof et al., 1992; Pujic et al., 2008). Each pipette contained a mixture of $1 \mu\text{M}$ Texas Red dextran to visualize the gradient and a specific guidance cue ($1 \mu\text{g/ml}$ BDNF; $900 \mu\text{g/ml}$ slit2 or $100 \mu\text{g/ml}$ netrin-1 in 0.1% DMSO). Different molecular weight dextrans were utilized depending on the guidance cue. This is to account for the fact that differently sized molecules travel distinctly once expelled into the medium (Pujic et al., 2008). For experiments involving BDNF, 10 kD dextran was used, and for experiments involving slit2 and netrin-1, 70 kD dextran was used. Micropipettes were then connected to a Picospritzer pressure application system (Parker, Hollis, NH). The injection rate was controlled by a Grass pulse generator (Natus Medical Incorporated, Pleasanton, CA) set to 1 Hz with 10 ms duration and 20 ms delay. Micropipettes were then positioned into the open chamber with cultured RGC neurons using a Patchman NP-2 micro-manipulator (Eppendorf, Hauppauge, NY). The angle between the pipette and the petri dish floor was adjusted and maintained at approximately 35° for all experiments. The position of the micropipette tip was maintained at approximately $25 \mu\text{m}$ above the cover glass and $100 \mu\text{m}$ away from the growth cone. Stable gradients could be created in less than one min from the initial pulse and sustained. To characterize the gradient, a fluorescent line scan was performed by placing one end of the line at the tip of the micropipette and the other at the growth cone to determine the approximate guidance cue concentration at the location of the growth cone. Cells were grown as previously described and transferred to a custom-made open chamber with serum-free media. Cells meeting specific criteria (i.e., axon length $> 15 \mu\text{m}$ and growing at a $45^\circ \pm 10^\circ$ angle to the pipette; visible growth cone;

no cells or debris in the way of the pipette/gradient) were then located and marked using MetaMorph 7.8 software. Only GFP-positive cells with axons were used as RGC neurons. The stable fluorescent dextran gradient was imaged and was periodically confirmed throughout each experiment. The cells were imaged at 0, 15, 30, 45, and 60 min. At 30 min, the medium was exchanged with new medium to prevent pH changes. The angle between the axis of growth at time = 0 min and time = 60 min was determined as an indicator of growth cone turning for experiments involving CST as Nox inhibitor. In the case of VAS2870, the growth cone response time was reduced to 30 min.

2.7 | Whole-mount antibody staining

After collection, embryos were kept in E3 media for 23 h, and media were exchanged to fish water with 0.003% of phenylthiourea (PTU_ (Sigma-Aldrich, St. Louis, MO) to inhibit melanization (Li et al., 2012). Embryos were anesthetized in 0.016% of tricaine methanesulfonate (Sigma-Aldrich, St. Louis, MO) and fixed overnight in 4% of paraformaldehyde (PFA)/ $1\times$ phosphate-buffered saline (PBS) at 4°C . Embryos were then washed with PBT ($1\times$ PBS, 0.5% Triton X-100) at RT. Next, samples were incubated in prechilled acetone for $30\text{--}75 \text{ min}$, depending on age, at -20°C . They were then washed in PBT at RT before incubation with $10 \mu\text{g/ml}$ proteinase K at RT (Sigma Aldrich, St. Louis, MO). Proteinase K digestion times ranged from 10 to 40 min depending on the age of the samples. Embryos were then fixed in 4% of PFA/ $1\times$ PBS for 30 min and washed extensively in PBT. Samples were then incubated with blocking solution (10% goat serum in PBT; Sigma) for 2 h at RT. The monoclonal zn-8 antibody raised against *alcalama* (zn-8; Zebrafish International Resource Center [ZIRC], Eugene, OR; RRID: AB10013774) was used as a primary antibody. Samples were incubated in zn-8 antibody diluted in $1:500$ blocking solution overnight at 4°C . The following day, they were washed in PBT, and the secondary antibody, goat anti-mouse IgG Alexa Fluor 488 (Thermo Fisher Scientific, Cat# A-11017, RRID:AB_2534084; Rockford, IL), was diluted $1:500$ in blocking solution. Samples were incubated overnight in secondary antibody solution at 4°C . The following day, the nuclear counterstain diamidino-2-phenylindole (Thermo Fisher Scientific, Cat# D1306, RRID:AB_2629482; Rockford, IL) was added to the secondary antibody solution at a $1:500$ dilution and incubated 1 h at RT. Next, samples were washed extensively with PBT and stored at 4°C in the dark until imaging.

Immunolabeled samples were mounted on glass-bottom dishes in 1% low-melting point agarose dissolved in $1\times$ PBS. Samples were oriented ventrally for OC and dorsally for OT imaging. The glass-bottom dish was filled with

1 × PBS prior imaging. Z-stacks were collected at 2 μm intervals using a Zeiss LSM 710 inverted scanning confocal microscope equipped with a 40X LD C-Apochromat 1.1 numerical aperture (NA) W Corr M27 objective (Zeiss). Figure panels showing zn-8 labeling are maximum intensity projections, whereas composite panels show a single optical section for DAPI (Figure 4). Maximum intensity projections were created using ImageJ software (ImageJ, RRID:SCR_003070). Two areas were measured: neuropil, which is the most intense area stained (yellow dashed line), and OT area, which includes all terminal axons (red dashed line) as outlined in Figure 4.

2.8 | H₂O₂ imaging and quantification using roGFP2-Orp1

The roGFP2-Orp1 construct was received from Dr. Tobias Dick (DKFZ, Germany) and subcloned into pCS2 + vector by the lab of Dr. Qing Deng (Purdue University). The roGFP2-Orp1 mRNA was transcribed from pCS2 + vector using mMessage mMachine SP6 kit (Thermo Fisher Scientific, Cat# AM1340, Waltham, MA). One nanoliter of 100 ng/μl mRNA was injected into one cell-stage embryos, which were incubated at 28°C until they reached the desired stage. For in vitro imaging, embryos with GFP signal were preselected and used for dissociated neuronal cultures as described above. Cultured RGC neurons were imaged using a TE2000 Eclipse microscope, a 60X 1.4 NA oil objective (Nikon), and an iXon Ultra 888 EM CCD camera (Andor). roGFP2-Orp1 was excited with 405/20 and 480/30 nm excitation filters and corresponding emission was acquired at 535/30 nm using the dichroic mirror 505DCXR (R400/15 and 480/30 nm, T510–700 nm; Chroma). Before imaging, the growth medium was replaced with serum-free, phenol red-free medium. Images were taken sequentially for each neuron before and 30 min after the control (PBS) or 10 μg/ml slit2 treatment to assess H₂O₂ levels. These images were analyzed with ImageJ software (ImageJ, RRID:SCR_003070). After average background subtraction, the 405 nm image was divided pixel-by-pixel by the 480 nm image in order to get 405/480 ratio image, which is representative of H₂O₂ levels. Measurements were done in the growth cone region, outlined by free-hand tool based on the DIC image, and averaged in the region of interest.

2.9 | Statistical analysis

Data sets were analyzed using GraphPad Prism software version 8.4.2 (GraphPad Prism, RRID:SCR_002798; La Jolla, CA). All raw data were assessed for normality using the D'Agostino–Pearson omnibus test included in GraphPad,

where applicable ($n \geq 8$). For $n < 8$, Shapiro–Wilk test was used to assess normality. Outliers were automatically identified and removed using the ROUT algorithm with a Q -value of 1%. For data sets containing two groups, Student's t test (two-tailed) or Mann–Whitney U test were used to identify differences among means, depending on the sample distribution. Data sets containing three or more groups, one-way ANOVA or Kruskal–Wallis test were used to identify differences among means. If a significant difference was detected with the ANOVA, the Tukey HSD method was used for multiple comparisons among groups. If a significant difference was detected in Kruskal–Wallis test, Dunn's multiple comparisons test was used. p values $< .05$ were considered significant. Graphs in Figures 1–4 and supplementary figures show mean \pm standard error of the mean for each group. Data are averaged from at least two independent experiments.

3 | RESULTS

3.1 | Nox inhibition abolishes slit2-mediated growth cone collapse

We have recently found that pan-isoform Nox inhibition using celastrol (CST) (Jaquet et al., 2011) between 32 and 36 hpf alters retinotectal pathfinding in embryonic zebrafish (Weaver et al., 2018). To determine whether Nox-derived ROS may play a cell-autonomous role in responses of zebrafish RGCs to cues involved in retinotectal pathfinding, we applied slit2, netrin-1, and BDNF to cultured RGC neurons in serum-free medium for 30 min, either in the presence of 0.1% DMSO (control) or 0.05 μM CST (Figure 1a). This low concentration of CST did not significantly affect axonal growth rate on its own and was previously determined through a dose-response curve (Weaver et al., 2018). As expected, slit2 application resulted in significantly reduced outgrowth rates (0.7 ± 3.1 μm/h, $*p = .036$) and increased growth cone collapse ($41.1 \pm 4.7\%$, $*p = .013$) as compared to control solution (11.9 ± 2.1 μm/h; $18.7 \pm 3.7\%$; Figure 1a-a''). However, when Nox was inhibited with 0.05 μM CST, we found that the average growth rate in the presence of slit2 increased (8.6 ± 2.9 μm/h; $p = .690$), and the percentage of growth cone collapse induced by slit2 returned to near control levels ($19.3 \pm 3.1\%$; $*p = .027$; Figure 1a''). Furthermore, slit2 increased the percentage of retracting axons (DMSO 21%, CST 23%; slit2 53%), whereas combined Nox inhibition reversed this effect (19%), suggesting a role of Nox in slit2-mediated retraction of RGC axons (Figure S1a; Table S1). RGCs treated with netrin-1 and BDNF showed growth rates similar to those of control-treated RGCs. However, when 0.05 μM CST was applied to the bath, we saw that the axonal growth rates of RGCs exposed to netrin-1 were significantly reduced

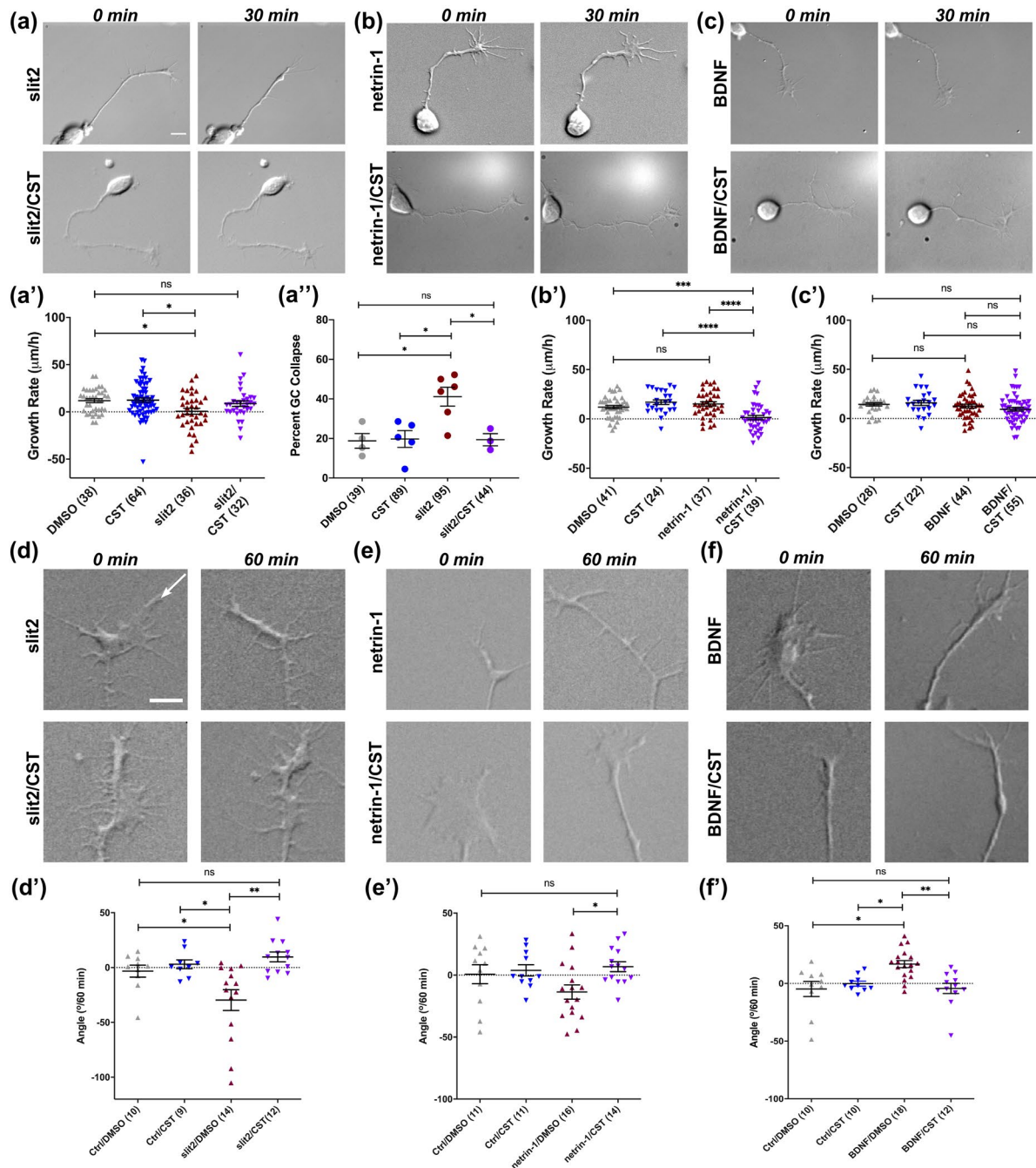


FIGURE 1 Nox inhibition abolishes slit2-mediated growth and guidance responses and regulates growth of netrin-1- and guidance of BDNF-treated RGCs. (a) Representative DIC images of RGC neurons from 34 hpf zebrafish embryos in serum-free medium before and after 30 min treated with 10 µg/ml slit2 in medium with 0.1% of DMSO (upper panel) and slit2 with 0.05 µM of CST (lower panel). (b–c) Representative DIC images of RGC neurons treated the same way as panel (a), with 0.1 µg/ml netrin-1 (b) and 0.01 µg/ml BDNF (c). Scale bar = 10 µm. (a'–c') Quantification of axonal growth rate (µm/h) of cells exposed to DMSO, CST, cue (slit2, netrin-1, or BDNF) and DMSO, or cue and CST. (a'') Percent growth cone collapse in response to slit2 and slit2/CST treatment, calculated from at least three independent experiments. (d–f) Representative DIC images depicting RGC growth cones in serum-free medium with 0.1% of DMSO right before cue gradient was applied (right panels) and the same growth cones after 60 min exposure to a cue gradient from the pipette (left panels). RGCs were exposed to gradients of slit2 (d), netrin-1 (e), or BDNF (f) in pipette without CST in the medium (upper panels) or with 0.05 µM CST in the medium (lower panels). The direction of the pipette is indicated by the white arrow in (d). Scale bar = 5 µm. (d'–f') Quantification of growth cone turning angle within 60 min of application of control buffer (Ctrl) without (Ctrl/DMSO) or with 0.05 µM celastrol (Ctrl/CST) in the medium or application of slit2 (d'), netrin-1 (e'), and BDNF (f') without or with CST in the medium. *n*-value indicates number of cells (one growth cone per cell). Each graph represents the average turning angle ± SEM. Data are averaged from at least three independent experiments. One-way ANOVA, post hoc Tukey test (a'', b', c', e'); Kruskal–Wallis, Dunn's Multiple Comparison's test (a', d', f'); **p* < .05; ***p* < .01, ****p* < .001, *****p* < .0001

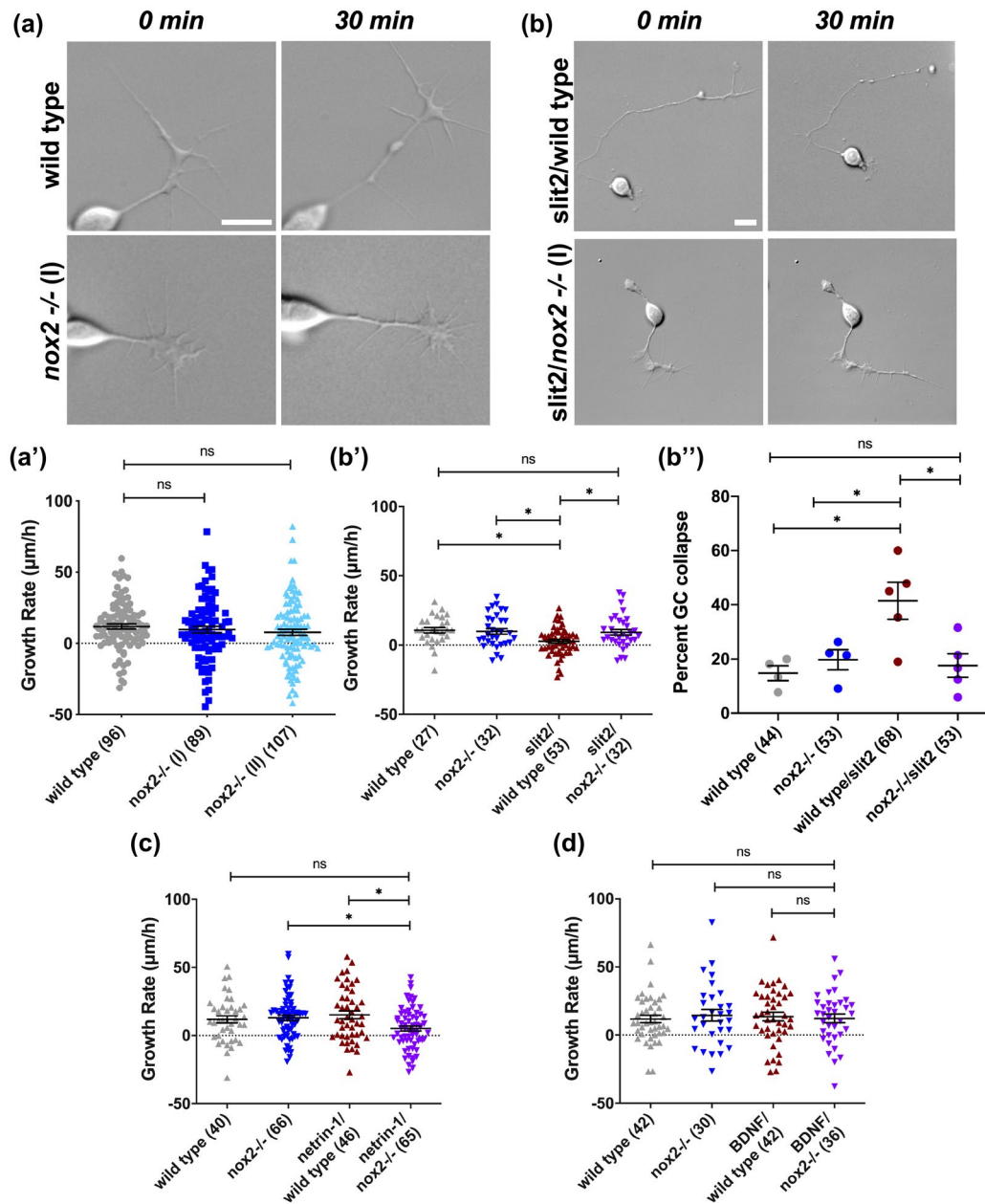


FIGURE 2 RGCs from *nox2*^{-/-} fish exhibit deficient growth responses to slit2 and netrin-1. (a) DIC image of a wildtype RGC before and after 30 min in serum-free medium (upper panel) and DIC image of an RGC neuron derived from a *nox2*^{-/-} (guide RNA I) zebrafish embryo before and after 30 min (lower panel). (a') Graph of axonal growth rates of RGC neurons derived from wildtype and *nox2*^{-/-} (guide RNA I and II) LOF mutants. (b) DIC image of a wildtype RGC neuron before and after 30 min treatment with 10 μ g/ml slit2, showing axonal retraction (upper panel). DIC image of *nox2*^{-/-} RGC before and after 30 min treatment with 10 μ g/ml slit2 (lower panel). The axon continued to grow despite the presence of slit2. (b', c, d) Quantification of axonal growth rates of wildtype and *nox2*^{-/-} (guide RNA I) RGCs with and without slit2 (b'), netrin-1 (c), or BDNF (d). (b'') Percent growth cone collapse in wildtype and *nox2*^{-/-} with or without slit2 treatment. Each graph represents the average axonal growth rate (b', c, d) percent growth cone collapse (b'') \pm SEM; *n*-value in parenthesis indicates the number of cells (b', c, d) or experiments (b'') analyzed. Scale bar = 10 μ m. Error bars denote average values \pm SEM; one-way ANOVA, post hoc Tukey test; **p* < .05

(1.4 ± 2.2 μ m/h) compared to the RGCs that were exposed to netrin-1 alone (15.1 ± 2.1 μ m/h; *****p* < .0001; Figure 1b-b'). Nox inhibition did not alter the growth rates of BDNF-treated RGC axons (Figure 1c-c'), whereas netrin-1 and BDNF did not alter the portion of axons with negative growth rates. When netrin-1 and BDNF were

applied together with CST, the percentage of retracting axons increased (Figure S1b,c; Table S1).

Although CST is one of the best pharmacological Nox inhibitors with respect to known off-target effects, we wanted to confirm our experimental results shown in Figure 1 with another inhibitor. We used VAS2870 (VAS; Figure S2),

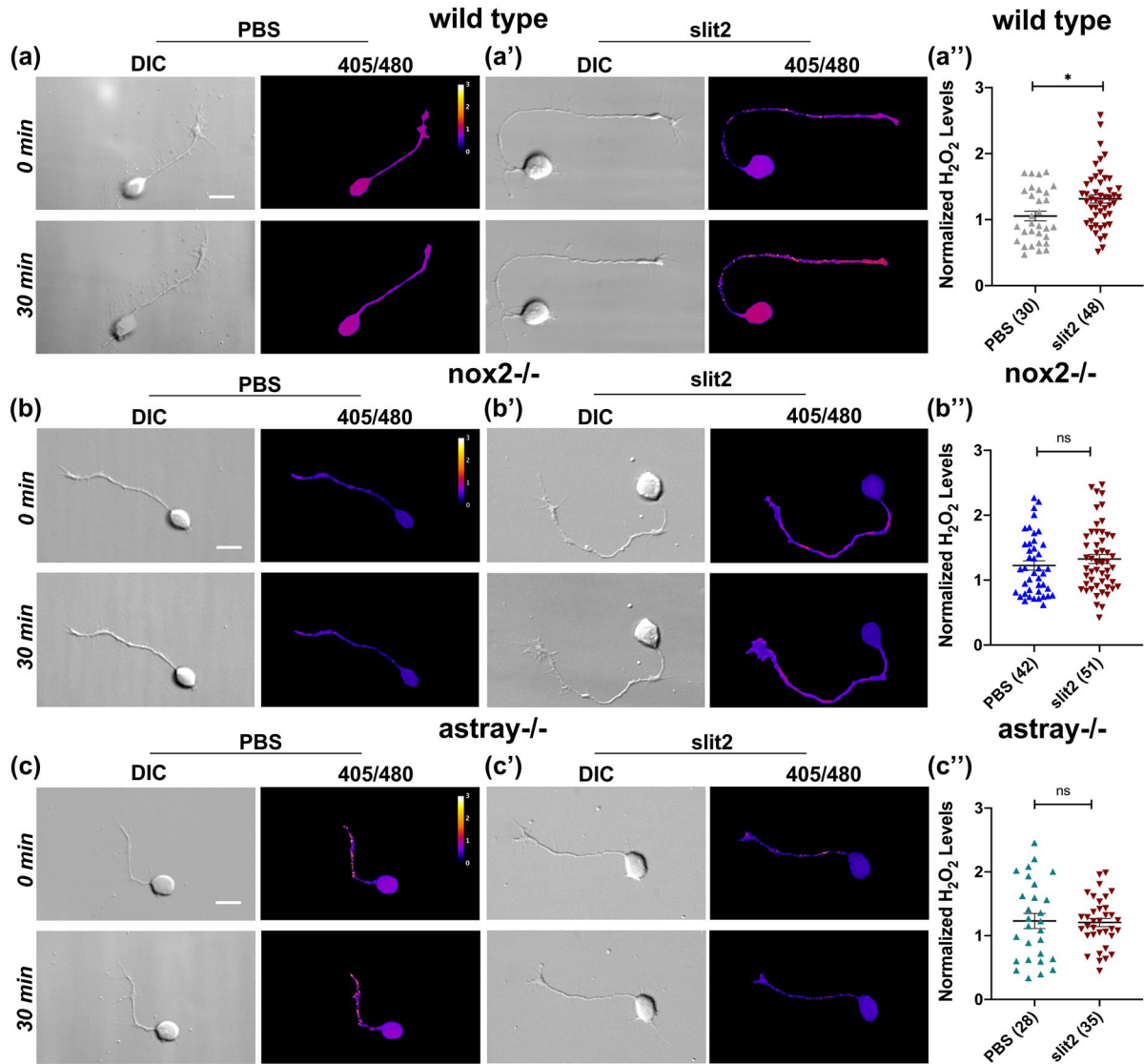


FIGURE 3 Slit2 causes an increase in intracellular H₂O₂ levels in wildtype RGCs, but not in *nox2*^{-/-} or *astray*^{-/-} RGCs. (a) DIC and 405/480 ratio images of wildtype RGCs before (upper panel) and after 30 min (lower panel) of control (PBS) treatment. (a') DIC and 405/480 ratio images of wildtype RGCs before (upper panel) and after 30 min (lower panel) of slit2 treatment. (b–b') DIC and 405/480 ratio images of *nox2*^{-/-} RGCs before (upper panel) and after 30 min (lower panel) of control (PBS) (b) and slit2 (b') treatment. (c–c') DIC and 405/480 ratio images of *astray*^{-/-} RGCs before (upper panel) and after 30 min (lower panel) of control (PBS) (c) and slit2 (c') treatment. Colors in the images represent original 405/480 ratio values (not normalized). (a''–c'') Quantification of intracellular H₂O₂ levels at the growth cones measured as the average intensity in the 405/480 ratio images in RGC growth cones. 405/480 ratios were normalized to corresponding before treatment (0 min) ratio values for each condition; thus, the values in the graphs are not on the same scale as the values in the images. Data are shown as mean ± SEM; *n*-value in parenthesis indicates the number of cells analyzed. Scale bar = 10 μm. Mann–Whitney *U* test (a'', b''), Two-tailed Student's *t* test (c''); **p* < .05

another relatively specific Nox inhibitor; however, it is known that it can also inhibit ryanodine receptors (Altenhöfer et al., 2015; Sun et al., 2012; ten Freyhaus et al., 2006). We applied 0.5 μM VAS in the medium, a concentration, which when presented alone did not significantly affect axonal growth rate (Figure S2a–c) as determined by a dose-response curve (Weaver et al., 2018). Similar to CST, we found that the decreased axonal growth rates in response to slit2 (-2.4 ± 1.5 μm/h; *****p* < .0001) returned to control values by the addition of VAS (10.5 ± 1.2 μm/h; *****p* < .0001;

Figure S2a). Similarly, as observed with CST, the growth rate in the presence of netrin-1 was reduced by combined treatment with VAS2870 (3.1 ± 1.0 μm/h; ***p* = .005; Figure S2b). In contrast to CST treatment (Figure 1c), VAS treatment significantly reduced growth rates when treated together with BDNF (1.5 ± 1.1 μm/h; *****p* < .0001; Figure S2c). The results with VAS2870-treated RGCs were generally similar to those with CST-treated neurons, suggesting that Nox activation is critical in these responses (Figure S2a–c). However, we noted one important difference between the two inhibitors

with respect to the BDNF-mediated growth. When VAS was used to inhibit Nox, growth rates in BDNF were reduced; this was not the case for CST. This difference could be due to the fact that VAS2870 has known off-target effects on ryanodine receptors, which control the release of calcium from intracellular stores (Sun et al., 2012). Intracellular calcium release has previously been shown to be an important signaling event of BDNF-mediated growth of zebrafish spinal neurons (Chen et al., 2013). Thus, the fact that VAS, but not CST-reduced BDNF-mediated growth, could be explained by the potential inhibition of ryanodine receptors by VAS2870.

In summary, these results show that pharmacological Nox inhibition abolishes the negative slit2-mediated RGC growth cone responses, whereas baseline growth rates on laminin substrate were not affected by low doses of Nox inhibitors. Netrin-1 (and BDNF in the case of VAS2870) lowered axonal outgrowth rates when combined with low doses of Nox inhibitors, suggesting that Nox may play distinct roles in axonal retraction mediated by different cues. Finally, the *in vitro* data further show that the role of Nox in cue-mediated growth is cell-autonomous.

3.2 | Growth cone guidance responses of RGC neurons are Nox-dependent

To determine whether Nox plays a role in mediating RGC growth cone responses to guidance cues, we performed a classical growth cone turning assay involving a micropipette filled with a soluble cue (Lohof et al., 1992; Pujic et al., 2008). When a buffer control solution (Ctrl) without cue was expelled from the pipette, RGC growth cones did not exhibit a preferred turning angle in either DMSO- or CST-containing mediums (Figure 1d-f'). As expected, RGC growth cones were repelled by slit2 gradients ($-29.7^\circ \pm 9.5^\circ$; Figure 1d,d'); however, when CST was present in the bath, this effect was eliminated ($9.7^\circ \pm 4.5^\circ$, $**p = .002$; Figure 1d,d'). In agreement with earlier studies (Hopker et al., 1999), the RGCs growing on laminin were repelled by netrin-1 ($-13.6^\circ \pm 5.7^\circ$), although the turning angle was not significantly different from control solution ($0.7^\circ \pm 7.6^\circ$, $p = .282$; Figure 1e,e'). However, when Nox was inhibited with CST, the trend toward repulsive growth cone turning by netrin-1 was eliminated ($6.8^\circ \pm 4.0^\circ$, $*p = .039$; Figure 1e'). RGC growth cones were attracted toward a BDNF gradient ($16.8^\circ \pm 3.0^\circ$, $*p = .025$; Figure 1f,f'); however, when CST was applied in the bath, this effect was eliminated ($-4.3^\circ \pm 4.4^\circ$, $**p = .002$; Figure 1f,f'). Finally, slit2- and BDNF-mediated growth cone guidance responses were also eliminated by application of 0.5 μM VAS in the medium (Figure S2d-f; the average turning angles were not as large as in the CST experiments shown in Figure 1, because gradients were only applied for 30 min VAS2870 experiments).

In summary, these results show that pharmacological Nox inhibition eliminates slit2-, netrin-1-, and BDNF-mediated growth cone turning *in vitro*, indicating that Nox activation is critical in these specific axonal guidance responses.

3.3 | Slit2- and netrin-1-mediated axonal growth responses are Nox2-dependent

Our results with pharmacological inhibitors suggest a role for Nox activity in growth and guidance responses to specific molecular cues; however, these inhibitors cannot distinguish among individual Nox isoforms and may have potential off-target effects, such as in the case of VAS2870 (Altenhöfer et al., 2015; Jaquet et al., 2011; Sun et al., 2012; ten Freyhaus et al., 2006). Therefore, to confirm our results and to identify the specific Nox isoform involved, we analyzed outgrowth of cultured RGC neurons derived from *nox2*^{-/-} loss of function (LOF) mutant fish. The *nox2*^{-/-} LOF fish line exhibits pathfinding errors during development of retinotectal connections (Weaver et al., 2018).

First, we compared the axonal growth rates of both *nox2*^{-/-} LOF mutant fish lines created with guide RNAs I and II to wildtype neurons (Figure 2a,a'). Wildtype RGCs exhibited an average growth rate of $11.9 \pm 1.8 \mu\text{m/h}$ (Figure 2a'). RGCs from both types of LOF mutants showed slightly reduced growth rates ($9.7 \pm 2.3 \mu\text{m/h}$ for *nox2*^{-/-} (type I gRNA) and $7.8 \pm 2.2 \mu\text{m/h}$ for *nox2*^{-/-} (type II gRNA), respectively); however, these differences were not statistically significant. Furthermore, we did not observe morphological differences *in vitro* between wildtype and mutant RGCs created by either type of guide RNA. Areas of cell bodies and growth cones as well as axonal lengths were comparable between wildtype and *nox2*^{-/-} (type I gRNA) RGCs (Figure S3). Due to the facts that the *nox2*^{-/-} fish generated with guide RNA I are predicted to produce a more severely truncated Nox2 protein than mutant fish generated using guide RNA II and that the phenotypes of these two mutant fish are comparable, we decided to focus the rest of our studies on the homozygous *nox2*^{-/-} (I) line, which we refer to as *nox2*^{-/-} hereafter. Furthermore, Nox2-p22phox association is required for plasma membrane targeting of the Nox2 catalytic core (Beaumel et al., 2014; Leto et al., 2009). The *nox2*^{-/-} (type I gRNA) lacks the binding region for p22phox, whereas the binding region is intact in the case of the *nox2*^{-/-} (type II gRNA) mutation. Hence, we do not expect the truncated Nox2 protein encoded by *nox2*^{-/-} (type I gRNA) mutated gene to be located at the plasma membrane.

Next, we tested whether growth rates in response to slit2, netrin-1, and BDNF are affected in *nox2*^{-/-} RGCs when compared to wildtype RGCs (Figure 2b-d). Consistent with our Nox inhibition results in Figure 1 and Figures S1 and S2, we found that the negative effect of slit2 on axonal growth was

eliminated in the *nox2*^{-/-} RGCs ($9.4 \pm 2.1 \mu\text{m/h}$) when compared to wildtype neurons treated with slit2 ($2.7 \pm 1.4 \mu\text{m/h}$; $*p = .041$; Figure 2b'). Furthermore, slit2-induced growth cone collapse ($41.4 \pm 6.8\%$) was also eliminated in *nox2*^{-/-} RGCs ($17.6 \pm 4.3\%$, $*p = .015$; Figure 2b''). slit2-mediated axon retraction was eliminated in *nox2*^{-/-} RGCs, similar to the CST treatment (Figure S1d; Table S1). The axonal growth was reduced in netrin-1-treated *nox2*^{-/-} mutant RGCs ($5.1 \pm 1.9 \mu\text{m/h}$) as compared to wildtype RGCs treated with netrin-1 ($15.2 \pm 2.9 \mu\text{m/h}$; $*p = .011$; Figure 2c), conversely no significant differences were observed for BDNF treatment ($12.3 \pm 3.2 \mu\text{m/h}$ vs. $13.6 \pm 3.2 \mu\text{m/h}$; Figure 2d). The percentage of retracting axons was not affected in *nox2*^{-/-} RGCs in response to netrin-1 and BDNF (Figure S1e,f; Table S1). In conclusion, these results suggest that axonal growth responses of RGC neurons to slit2 and netrin-1, but not BDNF, are dependent on Nox2.

3.4 | Slit2 increases intracellular H₂O₂ levels in zebrafish RGC growth cones *in vitro*

To further investigate the functional relationship between slit2-mediated growth cone responses and Nox2 signaling, we tested the hypothesis that slit2 alters the intracellular H₂O₂ levels in RGC growth cones, presumably by Nox2 regulation. To measure H₂O₂ in growth cones, we used the genetically encoded H₂O₂-specific biosensor roGFP2-Orp1 (Gutscher et al., 2009). Using this biosensor, we have previously shown that zebrafish embryos and RGCs respond to changes in H₂O₂ real time both *in vivo* and *in vitro*, respectively (Weaver et al., 2018). roGFP2-Orp1 is a ratiometric biosensor that reports H₂O₂ levels by the ratio of 405/535 nm and 480/535 nm signals. We measured the H₂O₂ levels in RGCs before and 30 min after control or cue incubation. We found that the basal H₂O₂ levels in all genotypes tested were similar (Kruskal–Wallis Test, $p = .762$; data not shown). When wildtype RGCs were incubated with slit2, there was a significant increase in H₂O₂ levels at the growth cones (normalized H₂O₂ levels of 1.3 ± 0.06 ; $*p = .020$) compared to wildtype RGCs treated with PBS only (1.05 ± 0.07 ; Figure 3a-a''). However, the normalized H₂O₂ levels in *nox2*^{-/-} RGCs treated with slit2 (1.3 ± 0.07) were comparable to that of PBS-treated RGCs (1.2 ± 0.07 ; $p = .276$), suggesting the slit2-mediated H₂O₂ production in the growth cone requires functional Nox2 (Figure 3b-b''). Furthermore, we tested zebrafish *astray*^{-/-} mutants that are deficient in the slit2-receptor *robo2* gene (Fricke et al., 2001). Like *nox2*^{-/-}, *astray*^{-/-} RGCs did not exhibit slit2-mediated H₂O₂ production (slit2; 1.2 ± 0.06 vs. PBS; 1.2 ± 0.11 ; $p = .855$) (Figure 3c-c''). Overall, these data suggest that zebrafish RGCs respond to slit2 by increasing intracellular H₂O₂ through Nox2 activity *in vitro*.

3.5 | Partial loss of Nox2 and Robo2 combined alters tectal innervation *in vivo*

Next, we investigated the relationship between slit2/Robo2 and Nox2 pathways *in vivo*. *Astray* (Robo2) mutants have RGC axon pathfinding defects, including midline crossing and projection in the OT (Fricke et al., 2001; Hutson & Chien, 2002; Karlstrom et al., 1996). Similarly, *nox2*^{-/-} mutants have defects in OT innervation (Weaver et al., 2018). To address whether Nox2 and slit2/Robo2 are in the same signaling pathway controlling RGC pathfinding, we performed genetic interaction experiments *in vivo*. Genes that are in the same signaling pathway are typically not expected to show an enhanced phenotype in double homozygous knockouts or mutants when compared to individual gene knockouts/mutants. On the contrary, weak phenotypes produced by heterozygotes or weaker alleles of different genes in the same pathway can be enhanced when combined with each other (Gistelink et al., 2018; Iwanami et al., 2016). Here, we tested our hypothesis that Nox2 and Robo2 are in the same pathway with *astray/nox2* double heterozygous mutants along with individual heterozygous and homozygous mutants (Figure 4). The larvae were stained with zn-8 antibody, which recognizes the cell adhesion molecule ALCAM a in RGC axons, at 3 and 5 dpf to investigate the formation of the OC and innervation of the OT by RGC axons, respectively (Figure 4a). At 3 dpf, RGC axons from *nox2*^{-/-} embryos were not as confined to the ON, as in wildtype embryos, resulting in a wider ON, especially at the OC (Figure 4b). Similarly, *astray*^{-/-} embryos also exhibited wider ON along with pathfinding errors after crossing the OC, which is in agreement with previous reports (Fricke et al., 2001; Hutson & Chien, 2002; Xiao et al., 2011) (Figure 4b). We measured the thickness of the ON originating from one eye at the chiasm (shown as red line in Figure 4b). ON thickness from individual homozygous mutants was significantly different from wildtype, *nox2*[±], *astray*[±], and *astray/nox2*[±] (Figure 4d, Table 1). In all *nox2*[±], *astray*[±], and *astray/nox2*[±] embryos, we did not observe mistargeted RGC axons, either before or after midline crossing, and the ON thickness was not different in *astray/nox*[±] as compared to individual heterozygous mutants (Figure 4b,d; Table 1).

Next, we investigated the innervation of the OT in mid-brain, the final synaptic target of RGCs. RGC axons project into the tectal neuropil, where they synapse with the tectal neurons to relay information from retina to brain. We have previously reported that *nox2*^{-/-} mutants exhibit a diffuse innervation of the OT; however, we did not carry out a detailed quantification of this phenotype (Weaver et al., 2018). Here, we measured the neuropil (yellow dashed line) and OT areas (red dashed line), as outlined in Figure 4c. Since *nox2*^{-/-} mutants have drastic RGC axon innervation defects and do not exhibit a clearly defined OT and neuropil area that is quantifiable, we excluded this genotype from our

TABLE 1 Statistical analysis comparing individual genotypes with wild type littermates for measured ON thickness, OT, and neuropil areas

Genotype		ON thickness (μm)	OT area (μm^2)	Neuropil area (μm^2)
Wild type	Mean \pm SEM	13.31 \pm 0.3	11,419 \pm 360.1	5,939 \pm 234.1
	Significantly different from wild type?	No	No	No
	<i>p</i> value	>.9999	.4859	.7999
<i>nox2</i> \pm	Mean \pm SEM	13.15 \pm 0.3	10,471 \pm 385.6	5,460 \pm 279.5
	Significantly different from wild type?	No	No	No
	<i>p</i> value	>.9999	.4859	.7999
<i>nox2</i> $-/-$	Mean \pm SEM	21.96 \pm 1.7	N/A	N/A
	Significantly different from wild type?	Yes	N/A	N/A
	<i>p</i> value	.0154	N/A	N/A
<i>astray</i> \pm	Mean \pm SEM	13.66 \pm 0.3	11,839 \pm 403.3	6,182 \pm 289.1
	Significantly different from wild type?	No	No	No
	<i>p</i> value	.9994	.9496	.9792
<i>astray</i> $-/-$	Mean \pm SEM	17.02 \pm 0.7	11,001 \pm 454.8	5,640 \pm 328.0
	Significantly different from wild type?	Yes	No	No
	<i>p</i> value	.0016	.9505	.9557
<i>astray/nox2</i> \pm	Mean \pm SEM	12.72 \pm 0.2	8,631 \pm 389.7	4,571 \pm 326.6
	Significantly different from wild type?	No	Yes	Yes
	<i>p</i> value	.8499	<.0001	.0169

quantitative analysis. The *astray* \pm (11,839 \pm 403.3 μm^2) and *nox2* \pm (10,471 \pm 385.6 μm^2) individual heterozygous mutants did not show a difference in OT area compared to wildtype larvae (11,419 \pm 360.1 μm^2 ; Figure 4f, Table 1). However, the *astray/nox2* \pm double heterozygous mutants had significantly decreased OT innervation area compared to wildtype (8,631 \pm 389.7 μm^2 ; *****p* < .0001), *nox2* \pm (**p* = .016), *astray* \pm (*****p* < .0001), and *astray* $-/-$ (11,001 \pm 454.8 μm^2 ; ****p* = .001). The *astray/nox2* \pm RGCs also exhibited decreased neuropil innervation (4,571 \pm 326.6 μm^2) as compared to wildtype (5,939 \pm 234.1 μm^2 ; **p* = .017; Figure 4e, Table 1). The *astray* $-/-$ larvae did not show differences in overall OT area. However, mistargeted RGC axons were evident outside the tectal area in both *astray* $-/-$ (38% of larvae) and *astray/nox2* \pm (35% of larvae; Figure 4c, red arrows). We did not observe any RGC axons outside of OT in wildtype, *nox2* \pm and *astray* \pm tecta (Chi-square test, *****p* < .0001). Taken together, partial loss of Nox2 and Robo2 individually did not affect RGC innervation of the OT; however, when combined, partial loss of both genes affected retinotectal innervation in vivo.

4 | DISCUSSION

There is emerging evidence that ROS signaling plays a role in nervous system development and function (Bórquez

et al., 2016; Nayernia et al., 2014). Nox-derived ROS have been implicated in various aspects of neuronal development, including neural stem cell maintenance and neurogenesis (Terzi & Suter, 2020), neuronal differentiation (Suzukawa et al., 2000), cerebellar development (Coyoy et al., 2013; Olgún-Albuérne & Morán, 2015), neuronal polarity (Wilson et al., 2015), axonal growth (Munnamalai & Suter, 2009; Munnamalai et al., 2014), and pathfinding (Gauron et al., 2016; Weaver et al., 2018). Here, we provide the first evidence that growth and guidance responses to specific molecular cues (e.g., slit2; netrin-1; BDNF) are mediated by Nox2 activity in a cell-autonomous manner.

The formation of retinotectal connections is affected when Nox is inhibited pharmacologically as well as in *nox2* $-/-$ mutants (Weaver et al., 2018). Several axonal guidance molecules that guide RGC axons to the brain in a number of model systems, including zebrafish, have been identified (Erskine & Herrera, 2014; Kita et al., 2015). Following differentiation, RGCs send their axons into the optic fiber layer at the inner surface of the retina medially toward the optic disk. Studies in mice have shown that slit proteins are critical for keeping RGC axons in the optic fiber layer as they grow toward the optic disk (Thompson et al., 2006). Here, we have shown with cultured RGC neurons that the repulsive growth and guidance effects of slit2 on RGC axons depend on neuronal Nox activity, specifically Nox2 (Figures 1–3). When Nox is inhibited in developing zebrafish embryos in vivo,

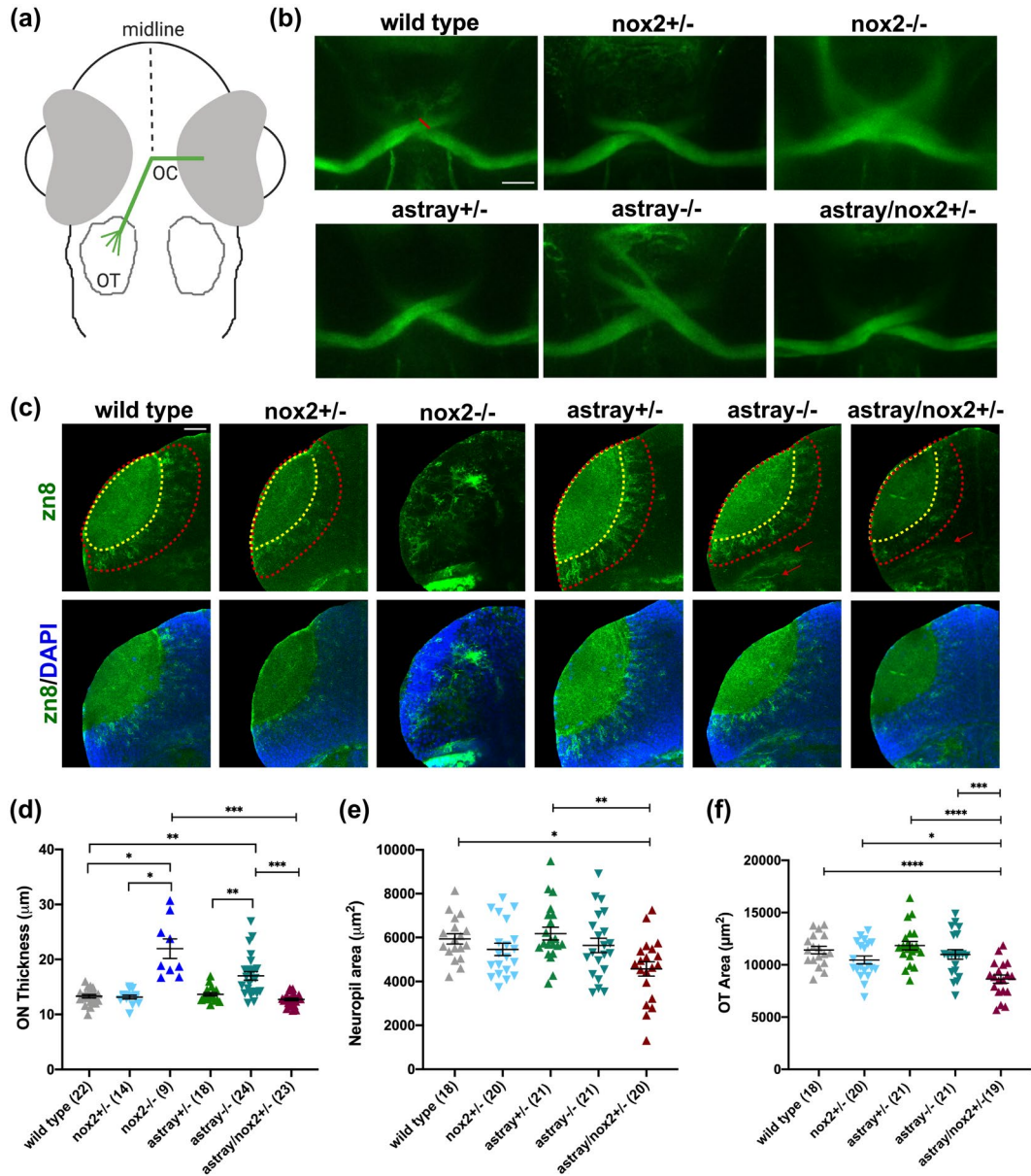


FIGURE 4 Combined partial loss of *Nox2* and *Robo2* alters RGC pathfinding in vivo. (a) Schematic presentation of zebrafish retinorectal pathway. RGCs (green) exit the eye as a single bundle ON, cross the midline forming OC and grow dorsally to the contralateral OT in the midbrain, where they make synaptic connections. (b) Ventral views of zn-8 staining from 3 dpf old embryos showing the OC. Measurements of ON thickness were done from single ON crossing the chiasm (red line). ON thickness from individual homozygous mutants (*nox2*^{-/-}, $21.9 \pm 1.7 \mu\text{m}$; *astray*^{-/-}, $17 \pm 0.7 \mu\text{m}$) were significantly different from wildtype ($13.3 \pm 0.3 \mu\text{m}$; vs. *nox2*^{-/-} * $p = .015$; vs. *astray*^{-/-} *** $p = .002$), *nox2*[±] ($13.1 \pm 0.3 \mu\text{m}$; vs. *nox2*^{-/-} * $p = .011$; vs. *astray*^{-/-} *** $p = .001$), *astray*[±] ($13.6 \pm 0.3 \mu\text{m}$; vs. *nox2*^{-/-} * $p = .015$; vs. *astray*^{-/-} *** $p = .006$), and *astray*/*nox2*[±] (12.7 ± 0.2 ; vs. *nox2*^{-/-} *** $p = .01$; vs. *astray*^{-/-} *** $p = .0002$). (c) Dorsal views of zn8 staining from 5 dpf old larvae showing the OT. Dashed red and yellow lines indicate the OT and neuropil areas, respectively, quantified in (e) and (f). Misguided RGC axons were evident in *astray*^{-/-} and *astray*/*nox2*[±] larvae outside the OT (red arrows). (d) Quantification of ON thickness. (e) Quantification of neuropil area. (f) Quantification of the OT area. Data are shown as mean \pm SEM; n -value in parenthesis indicates the number of embryos. Scale bar = 25 μm . Brown–Forsythe ANOVA, Dunnett's T3 multiple comparisons test (d); one-Way ANOVA/post hoc Tukey test (e,f); * $p < .05$; ** $p < .01$ *** $p < .001$, **** $p < .0001$. Comparisons were made across groups; nonsignificant results are not shown in graphs

the ganglion cell layer becomes wider (Weaver et al., 2018). This widening of the ganglion cell layer may be caused by an increased number of RGCs or by splayed axons in the optic fiber layer due to reduced slit2-mediated repulsion. Thus, our

results are consistent with a Nox-dependent role of slit2 signaling of RGC axons in intraretinal pathfinding.

Next, RGC axons need to exit the eye at the optic disk. Neuroepithelial cells surrounding the area of the optic disk

secrete netrin-1, which binds its receptor DCC on RGC growth cones causing local steering through the optic disk (Deiner et al., 1997). On laminin substrate, netrin-1 has repulsive effects on RGC growth cones (Hopker et al., 1999), which could explain how the growth cones are driven through the optic disk through a combination of local netrin-1 and laminin-mediated signaling (Erskine & Herrera, 2014). Here, we found that netrin-1 itself does not enhance RGC axon growth (Figures 1 and 2). However, when Nox was inhibited either pharmacologically or genetically, the RGC axon growth rates decreased with netrin-1. Furthermore, the netrin-mediated growth cone repulsion was abolished when Nox enzymes were inhibited, suggesting that the Nox activity is required for netrin-1-mediated RGC guidance. Additionally, Netrin-1-DCC pathway has previously shown to interact with slit-Robo2 pathway. For instance, Robo activation ceases the attractiveness to netrin-1 by binding to DCC after midline crossing in mammalian commissural axons (Stein & Tessier-Lavigne, 2001). Moreover, slit-Robo2 signaling suppresses attractive netrin-1 signal for proper anterior commissure and supraoptic tract formation during zebrafish anterior telencephalic neuron development (Zhang et al., 2012). Thus, it will be interesting to investigate whether such interaction occurs during different stages of RGC guidance involving Nox activity. Overall, we speculate that the proper channeling of RGC axons out of the eye and joining the optic tract requires Nox activation.

After exiting the eye, RGC axons soon face their next guidance decisions: The OC. Slit1/2-Robo signaling plays a crucial role in preventing pathfinding errors in the ON, in facilitating ventral midline crossing at the OC, and in formation of the optic tract (Fricke et al., 2001; Hutson & Chien, 2002; Plachez et al., 2008; Plump et al., 2002; Thompson, Barker, et al., 2006). We showed that Nox2 is required for slit2-mediated growth cone collapse, axonal growth inhibition, and retraction in vitro (Figures 1, 2; Figure S1). We speculate that slit2 might activate Nox2 to promote growth cone collapse. It has been previously shown that phorbol ester induces growth cone collapse and causes actin bundle loss; since phorbol esters act as protein kinase C (PKC) activators, one possible scenario is that Nox2 activation via PKC could promote growth cone collapse (Zhou & Cohan, 2001). Additionally, slit2 caused retraction in RGC axons in a Nox2-dependent manner (Figure S1a,d). Though netrin-1 and BDNF cause retraction only when Nox enzymes were inhibited with CST, this effect was not seen in *nox2*^{-/-} RGCs, suggesting that retraction could involve other Nox isoforms and that Nox could mediate and prevent retraction depending on the cue (Figure S1b,c,e,f). H₂O₂ has been shown to activate myosin II, as well as to increase F-actin flow rate and cell contractility in the lamella of nonneuronal cells (Anderson et al., 2008; Taulet et al., 2012). Furthermore, low amounts of H₂O₂ have been shown to promote contractile function and enhance

force generation, whereas high amounts inhibit contractile function in muscle fibers (Andrade et al., 1998). Thus, it is possible that different Nox isoforms could act with or against contractile machinery during growth cone guidance.

We also found that slit2 caused an increase in intracellular H₂O₂ levels in the RGC growth cones, which requires functional Nox2 and Robo2 (Figure 3). A stray mutants, which are deficient in Robo2, have major pathfinding defects, including axons diverging from ON and RGCs projecting outside the tectal area (Fricke et al., 2001; Hutson & Chien, 2002). We used *astray*^{ti272z} allele, which is the functional null mutation for Robo2, to investigate the relationship between Nox2 and slit2/Robo2 in vivo (Figure 4). As double homozygous *astray/nox2*^{-/-} have not been available for analysis so far, we investigated RGC guidance in double heterozygous mutants in addition to individual heterozygous and homozygous mutants. We speculated that if the Nox2 and Robo2 are in the same pathway, partial loss of functions would exhibit additive effects on RGC guidance. A subset of RGCs from *astray*^{-/-} embryos failed to cross midline properly and ended up projecting outside of OT (Figure 4b); a finding that has been previously reported (Fricke et al., 2001; Xiao et al., 2011). *nox2*^{-/-} RGCs also exhibited pathfinding errors at OC, as the ON thickened and did not remain a tight bundle. On the contrary, neither *astray*[±] and *nox2*[±], or *astray/nox2*[±] showed any such clear pathfinding errors near the OC. One possible explanation for this result could be that if only a few axons have pathfinding errors in double heterozygous mutants, the immunolabeling of all RGCs might hinder visualizing those mistargeted axons, as a result of the staining being too dense around OC. Although the in vivo results at the OC do not provide strong evidence, based on our in vitro results presented here, we speculate that a slit2/Robo2/Nox2 pathway regulates the correct RGC pathfinding at the OC.

Finally, RGC axons must project to their synaptic targets in the OT. RGCs mainly project to the neuropil, where they synapse with tectal neurons to create a topographic map of the visual field. Different RGCs project into specific sublamina to relay the visual information from the retina in a spatially controlled manner (Robles et al., 2013). In vivo experiments in *Xenopus* revealed that BDNF increases axonal arborization in the tectum, while decreasing dendritic arborization in the retina (Lom & Cohen-Cory, 1999). Furthermore, BDNF increases axonal outgrowth and branching of cultured rat RGC neurons in vitro (Bosco & Linden, 1999). Here, we found that BDNF-mediated attractive RGC growth cone turning is dependent on Nox activity, whereas BDNF-mediated axonal growth is not (Figures 1, 2; Figure S1). Furthermore, slit family proteins are also expressed in OT, and Robo2 has been shown to negatively regulate axon arbor formation (Campbell et al., 2007). slit1a, but not slit2, is required for proper laminar pathfinding of RGCs through Robo2 signaling in OT (Xiao et al., 2011). In the work presented here, we

found that both the total OT and neuropil area were decreased in double heterozygous *astray/nox2±* larvae compared to wildtype or single *astray±* and *nox2±* heterozygous mutant larvae (Figure 4). *nox2-/-* larvae had a strongly reduced OT innervation to a level where the OT was not clearly defined, preventing its measurement and quantification (Figure 4c). *astray-/-* larvae showed RGC pathfinding errors at the OC and outside the OT, but the OT and neuropil area itself was not significantly reduced (Figure 4c,e and f). Similar to *astray-/-* larvae, we also found RGCs projecting outside the OT in *astray/nox2±* larvae. Slit2/Robo2/Nox2 signaling directs RGC guidance at the OC resulting in pathfinding errors in mutants thereafter. However, in our study, we did not investigate the pathfinding of individual RGC axons, which, if further investigated, could reveal more details about the mutant phenotypes. Sparse labeling in *astray/nox2±* larvae could possibly glean new insights. Taken together, we propose that targeting RGC axons in the OT is Nox-dependent, possibly through mechanisms involving BDNF and slit1-2/Robo2/Nox2 signaling (Figure 5).

Our results with cultured RGC neurons strongly suggest that Nox2 acts cell-autonomously with respect to cue-mediated growth and guidance. Two important conclusions can be drawn from our findings. First, a small reduction of Nox activity does not significantly reduce baseline axonal growth rates on PDL/laminin but can have significant effects on cue-mediated axonal growth and guidance. Second, Nox2 seems to be the main Nox isoform mediating the observed growth and guidance effects following activation of guidance cue receptors, although it is possible that other Nox isoforms may be involved as well. Our in vivo data, on the contrary, do not provide direct proof that Nox2 acts cell-autonomously in RGC pathfinding, because experiments were performed with larvae that are Nox2-deficient in all cells. There is the possibility that part of the severe OT innervation defects of *nox2-/-* larvae is due to RGC-independent effects. *nox2-/-* mutant larvae with a phenotype exhibit neuronal cell bodies in neuropil, which normally is devoid of cell bodies (Figure 4c). Hence, the altered RGC innervation of the OT in *nox2-/-* larvae could be caused not only by an axonal pathfinding

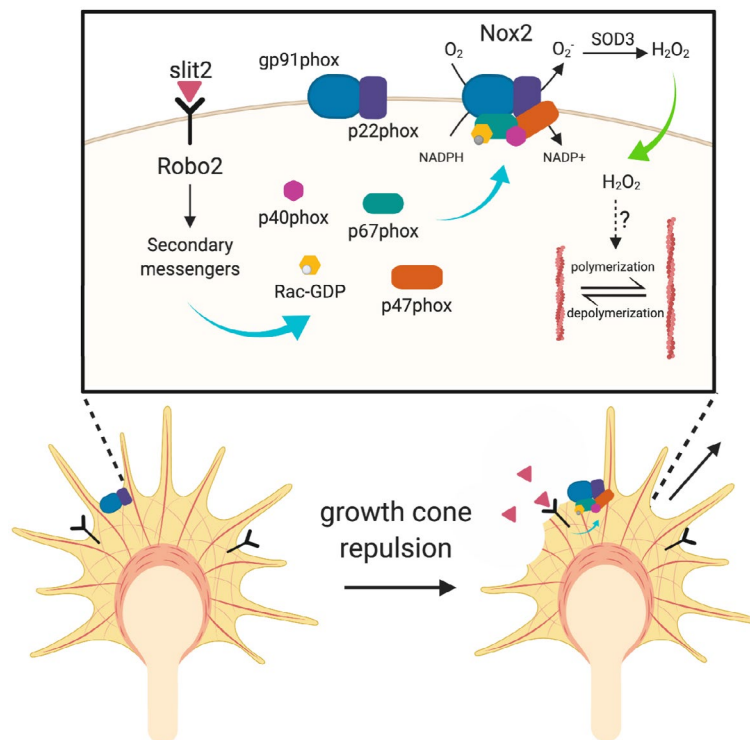


FIGURE 5 Proposed signaling pathway that involves slit2/Robo2 and Nox2 activation during retinotectal pathfinding. Schematic representation of the signaling events at the growth cone plasma membrane in response to slit2 is shown. From the data presented here, we propose that slit2-Robo2 interaction at the surface of RGC growth cones could initiate a signaling pathway that leads to activation of Nox2 via cytosolic subunits such as p47phox or Rac. Cytosolic subunits are translocated to the plasma membrane, where gp91phox-p22phox resides for a full activation of the enzyme complex. Once active, Nox2 transfers an electron from NADPH to molecular oxygen to produce superoxide, which is almost immediately converted to H_2O_2 either spontaneously or by extracellular dismutase enzyme (SOD3). H_2O_2 can either enter the cell through aquaporins to posttranslationally modify redox-sensitive proteins such as actin or oxidize receptor proteins extracellularly. The exact target(s) of H_2O_2 in this signaling pathway are not known in RGCs; however, there are multiple candidate redox-sensitive proteins that are involved in growth and guidance regulation. Upon target oxidation, a change in cytoskeletal dynamics cause growth cone collapse and repel the growth cone from slit2

defect of RGC neurons lacking Nox2, but also by an improper formation of the OT due to the lack of Nox2 in tectal cells. Thus, additional experiments will be required to test whether Nox2 has a cell-autonomous role in RGC pathfinding in vivo.

In conclusion and based on our results, we propose a pathway through which slit2/Robo2 activates Nox2 signaling in RGC growth cones to guide the RGC axons to the OT (Figure 5). When slit2 binds to its receptor Robo2 at the RGC growth cone surface, a signaling cascade is initiated. This signaling could induce secondary messengers that can potentially activate the cytosolic subunits of Nox2 complex. For instance, PKC can phosphorylate p47phox to remove its autoinhibition. Once phosphorylated, p47phox can bind to p67phox and assist its translocation to plasma membrane, where p67phox promotes the catalytic activity of Nox2. When fully activated, Nox2 generates superoxide, which is converted to H₂O₂ either spontaneously or by extracellular dismutase (SOD3) (Wang et al., 2018). H₂O₂ can then cross plasma membrane by simple diffusion or aquaporins, and as its half-life is longer than that other ROS, it can contribute to intracellular signaling (Bienert et al., 2006, 2007; Reczek & Chandel, 2015).

Any redox-sensitive protein in close proximity to H₂O₂, could be posttranslationally modified by H₂O₂. Here, we depicted actin as a possible target for oxidation. Nox-derived H₂O₂ was shown to alter actin polymerization in neutrophils during phagocytosis, participate in migration by modulating F-actin network in lamellipodium and lamella in epithelial cells, and rearrange actin in plants in innate immunity (Ryder et al., 2013; Sakai et al., 2012; Taulet et al., 2012). Another possible redox modification target for Nox-derived H₂O₂ are actin-binding/regulatory proteins. One particular candidate is actin-severing protein cofilin. It was shown that slit2 increases cofilin in the RGC growth cones by repressing the miRNA that negatively regulates cofilin translation (Bellon et al., 2017; Piper et al., 2006). Furthermore, cofilin is a redox-sensitive protein, and its oxidation interfered with its actin-binding (Cameron et al., 2015; Klamt et al., 2009) and its actin-severing activity (Klemke et al., 2008). Another important actin-regulatory protein is Rac1, which is also a part of Nox2 activation complex. Hence, Rac1 has a dual function with respect Nox2-mediated actin cytoskeleton regulation. Furthermore, Rac1 is a redox-sensitive protein, and Rac1-mediated Nox activation promotes further Rac1 activity (Wilson et al., 2016). Thus, signaling pathways might be working in cohort to coordinate the growth cone responses to slit2. Future studies identifying direct targets for Nox2-mediated H₂O₂ will shed light on specific signaling events in the growth cones of developing RGCs.

ACKNOWLEDGMENTS

This work was supported by the National Institute of Neurological Disorders and Stroke (Grant R01NS117701),

National Science Foundation (Grant 1146944-IOS), the Indiana Traumatic Spinal Cord and Brain Injury Research Fund (Grant 20000289), the Purdue Research Foundation (Grant 209911), and the Office of the Executive Vice President for Research and Partnerships at Purdue University (Grant 210362). We thank Dr. Yuk Fai Leung, Dr. Qing Deng, and Dr. Estuardo Robles for technical advice on this work. We thank Elisabeth Garland-Kuntz for establishing the growth cone turning assay, Tenaizus Woods, and Perapa Chotiprasidhi for helping with maintaining and genotyping Nox mutant fish lines. We thank Kenny Nguyen, Leah Biasi, and Saron Bhoopathy for their help in retinal ganglion cell culture experiments. We thank Deborah Bieseimer, Skye Brown, and George Stoner for managing the fish facility. We thank Dr. Tobias Dick (DKFZ, Germany) for providing the roGFP2-Orp1 construct and the lab of Dr. Qing Deng for providing us with roGFP2-Orp1 in pCS2 + vector. We thank Dr. Brian A. Link (Medical College of Wisconsin) for providing the *Tg(ath5:GFP)* transgenic line, and Dr. Michael Granato (University of Pennsylvania) for providing the *astray^{ti272z}* mutant line. We thank Gentry Lee for comments on the manuscript. Schematics in Figures 4 and 5 are created with Biorender.com.

CONFLICT OF INTEREST

The authors declare that they have no competing interests.

AUTHORS' CONTRIBUTIONS

AT, HR, CJW, and DMS designed the experiments. AT performed all in vivo experiments and in vitro H₂O₂ imaging. HR and performed the growth and guidance experiments with cultured RGC neurons. CJW established the RGC culture system and *nox2*^{-/-} mutant fish lines. AT, HR, and DMS wrote the manuscript. All authors discussed and edited the manuscript. All authors read and approved the final manuscript.

DATA AVAILABILITY STATEMENT

The data sets used and/or analyzed during the current study are available from the corresponding author on reasonable request.

ORCID

Aslihan Terzi  <https://orcid.org/0000-0003-3361-532X>

Daniel M. Suter  <https://orcid.org/0000-0002-5230-7229>

REFERENCES

- Acker, T., & Acker, H. (2004). Cellular oxygen sensing need in CNS function: Physiological and pathological implications. *Journal of Experimental Biology*, 207(18), 3171–3188. <https://doi.org/10.1242/jeb.01075>
- Altenhöfer, S., Radermacher, K. A., Kleikers, P. W. M., Wingler, K., & Schmidt, H. H. H. W. (2015). Evolution of NADPH oxidase

- inhibitors: Selectivity and mechanisms for target engagement. *Antioxidants & Redox Signaling*, 23(5), 406–427. <https://doi.org/10.1089/ars.2013.5814>
- Anderson, T. W., Vaughan, A. N., & Cramer, L. P. (2008). Retrograde flow and myosin II activity within the leading cell edge deliver F-actin to the lamella to seed the formation of graded polarity actomyosin II filament bundles in migrating fibroblasts. *Molecular Biology of the Cell*, 19, 5006–5018. <https://doi.org/10.1091/mbc.E08-01-0034>
- Andrade, F. H., Reid, M. B., Allen, D. G., & Westerblad, H. (1998). Effect of hydrogen peroxide and dithiothreitol on contractile function of single skeletal muscle fibres from the mouse. *Journal of Physiology*, 509(2), 565–575. <https://doi.org/10.1111/j.1469-7793.1998.565bn.x>
- Babior, B. M. (2004). NADPH oxidase. *Current Opinion in Immunology*, 16(1), 42–47. <https://doi.org/10.1016/j.coi.2003.12.001>
- Beaumel, S., Grunwald, D., Fieschi, F., & Stasia, M. J. (2014). Identification of NOX2 regions for normal biosynthesis of cytochrome b558 in phagocytes highlighting essential residues for p22phox binding. *Biochemical Journal*, 464(3), 425–437. <https://doi.org/10.1042/BJ20140555>
- Bedard, K., & Krause, K.-H. (2007). The NOX family of ROS-generating NADPH oxidases: Physiology and pathophysiology. *Physiological Reviews*, 87(1), 245–313. <https://doi.org/10.1152/physrev.00044.2005>
- Bellon, A., Iyer, A., Bridi, S., Lee, F. C. Y., Ovando-Vázquez, C., Corradi, E., Longhi, S., Rocuzzo, M., Strohbuecker, S., Naik, S., Sarkies, P., Miska, E., Abreu-Goodger, C., Holt, C. E., & Baudet, M.-L. (2017). miR-182 regulates slit2-mediated axon guidance by modulating the local translation of a specific mRNA. *Cell Reports*, 18(5), 1171–1186. <https://doi.org/10.1016/j.celrep.2016.12.093>
- Bienert, G. P., Møller, A. L. B., Kristiansen, K. A., Schulz, A., Møller, I. M., Schjoerring, J. K., & Jahn, T. P. (2007). Specific aquaporins facilitate the diffusion of hydrogen peroxide across membranes. *The Journal of Biological Chemistry*, 282(2), 1183–1192. <https://doi.org/10.1074/jbc.M603761200>
- Bienert, G. P., Schjoerring, J. K., & Jahn, T. P. (2006). Membrane transport of hydrogen peroxide. *Biochimica et Biophysica Acta*, 1758(8), 994–1003. <https://doi.org/10.1016/j.bbamem.2006.02.015>
- Bórquez, D. A., Urrutia, P. J., Wilson, C., Van Zundert, B., Núñez, M. T., & González-Billault, C. (2016). Dissecting the role of redox signaling in neuronal development. *Journal of Neurochemistry*, 137(4), 506–517. <https://doi.org/10.1111/jnc.13581>
- Bosco, A., & Linden, R. (1999). BDNF and NT-4 differentially modulate neurite outgrowth in developing retinal ganglion cells. *Journal of Neuroscience Research*, 57(6), 759–769. [https://doi.org/10.1002/\(SICI\)1097-4547\(19990915\)57:6<759::AID-JNRI>3.0.CO;2-Y](https://doi.org/10.1002/(SICI)1097-4547(19990915)57:6<759::AID-JNRI>3.0.CO;2-Y)
- Brandes, R. P., & Kreuzer, J. (2005). Vascular NADPH oxidases: Molecular mechanisms of activation. *Cardiovascular Research*, 65(1), 16–27. <https://doi.org/10.1016/j.cardiores.2004.08.007>
- Cameron, J. M., Gabrielsen, M., Chim, Y. H., Munro, J., McGhee, E. J., Sumpton, D., Eaton, P., Anderson, K. I., Yin, H., & Olson, M. F. (2015). Polarized cell motility induces hydrogen peroxide to inhibit cofilin via cysteine oxidation. *Current Biology*, 25(11), 1520–1525. <https://doi.org/10.1016/j.cub.2015.04.020>
- Campbell, D. S., Stringham, S. A., Timm, A., Xiao, T., Law, M.-Y., Baier, H., Nonet, M. L., & Chien, C.-B. (2007). Slit1a Inhibits retinal ganglion cell arborization and synaptogenesis via robo2-dependent and -independent pathways. *Neuron*, 55(2), 231–245. <https://doi.org/10.1016/j.neuron.2007.06.034>
- Cao, X., Demel, S. L., Quinn, M. T., Galligan, J. J., & Kreulen, D. (2009). Localization of NADPH oxidase in sympathetic and sensory ganglion neurons and perivascular nerve fibers. *Autonomic Neuroscience: Basic and Clinical*, 151(2), 90–97. <https://doi.org/10.1016/j.autneu.2009.07.010>
- Chaudhari, P., Ye, Z., & Jang, Y.-Y. (2014). Roles of reactive oxygen species in the fate of stem cells. *Antioxidants & Redox Signaling*, 20(12), 1881–1890. <https://doi.org/10.1089/ars.2012.4963>
- Chen, Z., Lee, H., Henle, S. J., Cheever, T. R., Ekker, S. C., & Henley, J. R. (2013). Primary neuron culture for nerve growth and axon guidance studies in Zebrafish (*Danio rerio*). *PLoS One*, 8(3), e57539. <https://doi.org/10.1371/journal.pone.0057539>
- Cooney, S. J., Zhao, Y., & Byrnes, K. R. (2014). Characterization of the expression and inflammatory activity of NADPH oxidase after spinal cord injury. *Free Radical Research*, 48(8), 929–939. <https://doi.org/10.3109/10715762.2014.927578>
- Coyoy, A., Olgún-Albuerno, M., Martínez-Briseno, P., & Moran, J. (2013). Role of reactive oxygen species and NADPH-oxidase in the development of rat cerebellum. *Neurochemistry International*, 62(7), 998–1011. <https://doi.org/10.1016/j.neuint.2013.03.009>
- De La Torre, J. R., Höpker, V. H., Ming, G. L., Poo, M. M., Tessier-Lavigne, M., Hemmati-Brivanlou, A., & Holt, C. E. (1997). Turning of retinal growth cones in a netrin-1 gradient mediated by the netrin receptor DCC. *Neuron*, 19(6), 1211–1224. [https://doi.org/10.1016/S0896-6273\(00\)80413-4](https://doi.org/10.1016/S0896-6273(00)80413-4)
- Deiner, M. S., Kennedy, T. E., Fazeli, A., Serafini, T., Tessier-Lavigne, M., & Sretavan, D. W. (1997). Netrin-1 and DCC mediate axon guidance locally at the optic disc: Loss of function leads to optic nerve hypoplasia. *Neuron*, 19(3), 575–589. [https://doi.org/10.1016/S0896-6273\(00\)80373-6](https://doi.org/10.1016/S0896-6273(00)80373-6)
- Dickinson, B. C., Peltier, J., Stone, D., Schaffer, D. V., & Chang, C. J. (2011). Nox2 redox signaling maintains essential cell populations in the brain. *Nature Chemical Biology*, 7(2), 106–112. <https://doi.org/10.1038/nchembio.497>
- Erskine, L., & Herrera, E. (2014). Connecting the retina to the brain. *ASN Neuro*, 6(6), 1–26. <https://doi.org/10.1177/1759091414562107>
- Erskine, L., Williams, S. E., Brose, K., Kidd, T., Rachel, R. A., Goodman, C. S., Tessier-Lavigne, M., & Mason, C. A. (2000). Retinal ganglion cell axon guidance in the mouse optic chiasm: Expression and function of robo and slits. *The Journal of Neuroscience*, 20(13), 4975–4982. <https://doi.org/10.1523/JNEUROSCI.20-13-04975.2000>
- Finkel, T. (2011). Signal transduction by reactive oxygen species. *The Journal of Cell Biology*, 194(1), 7–15. <https://doi.org/10.1083/jcb.201102095>
- Fricke, C., Lee, J., Geiger-Rudolph, S., Bonhoeffer, F., & Chien, C. (2001). *astray*, a Zebrafish roundabout Homolog required for retinal axon guidance. *Science*, 292(5516), 507–511. <https://doi.org/10.1126/science.1059496>
- Gauron, C., Meda, F., Dupont, E., Albadri, S., Quenech' Du, N., Ipendey, E., Volovitch, M., Del Bene, F., Joliot, A., Rampon, C., & Vrzi, S. (2016). Hydrogen peroxide (H₂O₂) controls axon pathfinding during zebrafish development. *Developmental Biology*, 414(2), 133–141. <https://doi.org/10.1016/j.ydbio.2016.05.004>
- Gistelincq, C., Kwon, R. Y., Malfait, F., Symoens, S., Harris, M. P., Henke, K., Hawkins, M. B., Fisher, S., Sips, P., Guillemyn, B., Bek, J. W., Vermassen, P., De Saffel, H., Witten, P. E., Weis, M. A., De Paepe, A., Eyre, D. R., Willaert, A., & Coucke, P. J. (2018). Zebrafish type I collagen mutants faithfully recapitulate human type I collagenopathies. *Proceedings of the National Academy of Sciences*, 115(12), 6345–6350. <https://doi.org/10.1073/pnas.1715000115>

- Sciences of the United States of America*, 115(34), E8037–E8046. <https://doi.org/10.1073/pnas.1722200115>
- Gutschner, M., Sobotta, M. C., Wabnitz, G. H., Ballikaya, S., Meyer, A. J., Samstag, Y., & Dick, T. P. (2009). Proximity-based protein thiol oxidation by H₂O₂-scavenging peroxidases. *Journal of Biological Chemistry*, 284(46), 31532–31540. <https://doi.org/10.1074/jbc.M109.059246>
- Halliwell, B. (1992). Reactive oxygen species and the central nervous system. *Journal of Neurochemistry*, 59(5), 1609–1623. <https://doi.org/10.1111/j.1471-4159.1992.tb10990.x>
- Hensley, M. R., & Leung, Y. F. (2010). A convenient dry feed for raising zebrafish larvae. *Zebrafish*, 7(2), 219–231. <https://doi.org/10.1089/zeb.2010.0652>
- Hilburger, E. W., Conte, E. J., McGee, D. W., & Tammariello, S. P. (2005). Localization of NADPH oxidase subunits in neonatal sympathetic neurons. *Neuroscience Letters*, 377(1), 16–19. <https://doi.org/10.1016/j.neulet.2004.11.066>
- Hopker, V. H., Shewan, D., Tessier-Lavigne, M., Poo, M., & Holt, C. (1999). Growth-cone attraction to netrin-1 is converted to repulsion by laminin-1. *Nature*, 401(6748), 69–73. <https://doi.org/10.1038/43441>
- Hu, M., & Easter, S. S. (1999). Retinal Neurogenesis: The formation of the initial central patch of postmitotic cells. *Developmental Biology*, 207(2), 309–321. <https://doi.org/10.1006/dbio.1998.9031>
- Hutson, L. D., & Chien, C. (2002). Pathfinding and error correction by retinal axons: The role of astray/robo2. *Neuron*, 33(2), 205–217. [https://doi.org/10.1016/s0896-6273\(01\)00579-7](https://doi.org/10.1016/s0896-6273(01)00579-7)
- Iwanami, N., Sikora, K., Richter, A. S., Mönnich, M., Guerri, L., Soza-Ried, C., Lawir, D.-F., Mateos, F., Hess, I., O'Meara, C. P., Schorpp, M., & Boehm, T. (2016). Forward genetic screens in zebrafish identify pre-mRNA-processing pathways regulating early T cell development. *Cell Reports*, 17(9), 2259–2270. <https://doi.org/10.1016/j.celrep.2016.11.003>
- Jaquet, V., Marcoux, J., Forest, E., Leidal, K. G., McCormick, S., Westermaier, Y., Perozzo, R., Plastre, O., Fioraso-Cartier, L., Diebold, B., Scapozza, L., Nauseef, W. M., Fieschi, F., Krause, K.-H., & Bedard, K. (2011). NADPH oxidase (NOX) isoforms are inhibited by celastrol with a dual mode of action. *British Journal of Pharmacology*, 164(2b), 507–520. <https://doi.org/10.1111/j.1476-5381.2011.01439.x>
- Karlstrom, R. O., Trowe, T., Klostermann, S., Baier, H., Brand, M., Crawford, A. D., & Bonhoeffer, F. (1996). Zebrafish mutations affecting retinotectal axon pathfinding. *Development*, 123, 427–438.
- Kastenhuber, E., Kern, U., Bonkowsky, J. L., Chien, C. B., Driever, W., & Schweitzer, J. (2009). Netrin-DCC, robo-slit, and heparan sulfate proteoglycans coordinate lateral positioning of longitudinal dopaminergic diencephalospinal axons. *Journal of Neuroscience*, 29(28), 8914–8926. <https://doi.org/10.1523/JNEUROSCI.0568-09.2009>
- Kimmel, C. B., Ballard, W. W., Kimmel, S. R., Ullmann, B., & Schilling, T. F. (1995). Stages of embryonic development of the zebrafish. *Developmental Dynamics*, 203(3), 253–310. <https://doi.org/10.1002/aja.1002030302>
- Kita, E. M., Scott, E. K., & Goodhill, G. J. (2015). Topographic wiring of the retinotectal connection in zebrafish. *Developmental Neurobiology*, 75(6), 542–556. <https://doi.org/10.1002/dneu.22256>
- Klamt, F., Zdanov, S., Levine, R. L., Pariser, A., Zhang, Y., Zhang, B., Yu, L.-R., Veenstra, T. D., & Shacter, E. (2009). Oxidant-induced apoptosis is mediated by oxidation of the actin-regulatory protein cofilin. *Nature Cell Biology*, 11(10), 1241–1246. <https://doi.org/10.1038/ncb1968>
- Klemke, M., Wabnitz, G. H., Funke, F., Funk, B., Kirchgessner, H., & Samstag, Y. (2008). Oxidation of cofilin mediates T cell hyporesponsiveness under oxidative stress conditions. *Immunity*, 29(3), 404–413. <https://doi.org/10.1016/j.immuni.2008.06.016>
- Leto, T. L., Morand, S., Hurt, D., & Ueyama, T. (2009). Targeting and regulation of reactive oxygen species generation by Nox family NADPH oxidases. *Antioxidants & Redox Signaling*, 11(10), 2607–2619. <https://doi.org/10.1089/ars.2009.2637>
- Li, Z., Ptak, D., Zhang, L., Walls, E. K., Zhong, W., & Leung, Y. F. (2012). Phenylthiourea specifically reduces zebrafish eye size. *PLoS One*, 7(6), e40132. <https://doi.org/10.1371/journal.pone.0040132>
- Lin, C.-C., Hsieh, H.-L., Shih, R.-H., Chi, P.-L., Cheng, S.-E., Chen, J.-C., & Yang, C.-M. (2012). NADPH oxidase 2-derived reactive oxygen species signal contributes to bradykinin-induced matrix metalloproteinase-9 expression and cell migration in brain astrocytes. *Cell Communication and Signaling*, 10(1), 35. <https://doi.org/10.1186/1478-811X-10-35>
- Lohof, A. M., Quillan, M., Dan, Y., & Poo, M. M. (1992). Asymmetric modulation of cytosolic cAMP activity induces growth cone turning. *The Journal of Neuroscience*, 12(4), 1253–1261. <https://doi.org/10.1523/JNEUROSCI.12-04-01253.1992>
- Lom, B., & Cohen-Cory, S. (1999). Brain-derived neurotrophic factor differentially regulates retinal ganglion cell dendritic and axonal arborization in vivo. *The Journal of Neuroscience*, 19(22), 9928–9938. <https://doi.org/10.1523/JNEUROSCI.19-22-09928.1999>
- Morinaka, A., Yamada, M., Itofusa, R., Funato, Y., Yoshimura, Y., Nakamura, F., Yoshimura, T., Kaibuchi, K., Goshima, Y., Hoshino, M., Kamiguchi, H., & Miki, H. (2011). Thioredoxin mediates oxidation-dependent phosphorylation of CRMP2 and growth cone collapse. *Science Signaling*, 4(170), ra26. <https://doi.org/10.1126/scisignal.2001127>
- Munnamalai, V., & Suter, D. M. (2009). Reactive oxygen species regulate F-actin dynamics in neuronal growth cones and neurite outgrowth. *Journal of Neurochemistry*, 108(3), 644–661. <https://doi.org/10.1111/j.1471-4159.2008.05787.x>
- Munnamalai, V., Weaver, C. J., Weisheit, C. E., Venkatraman, P., Agim, Z. S., Quinn, M. T., & Suter, D. M. (2014). Bidirectional interactions between Nox2-type NADPH oxidase and the F-actin cytoskeleton in neuronal growth cones. *Journal of Neurochemistry*, 130(4), 526–540. <https://doi.org/10.1111/jnc.12734>
- Nauseef, W. M. (2004). Assembly of the phagocyte NADPH oxidase. *Histochemistry and Cell Biology*, 122(4), 277–291. <https://doi.org/10.1007/s00418-004-0679-8>
- Nayernia, Z., Jaquet, V., & Krause, K.-H. (2014). New insights on NOX enzymes in the central nervous system. *Antioxidants & Redox Signaling*, 20(17), 2815–2837. <https://doi.org/10.1089/ars.2013.5703>
- Olguín-Albuerno, M., & Morán, J. (2015). ROS produced by NOX2 controls *in vitro* development of cerebellar granule neurons development. *ASN Neuro*, 7(2), 175909141557871. <https://doi.org/10.1177/1759091415578712>
- Piper, M., Anderson, R., Dwivedy, A., Weinl, C., van Horck, F., Leung, K. M., Cogill, E., & Holt, C. (2006). Signaling mechanisms underlying Slit2-induced collapse of *Xenopus* retinal growth cones. *Neuron*, 49(2), 215–228. <https://doi.org/10.1016/j.neuron.2005.12.008>
- Plachez, C., Andrews, W., Liapi, A., Knoell, B., Drescher, U., Mankoo, B., Zhe, L., Mambetisaeva, E., Annan, A., & Bannister, L. (2008). Robos are required for the correct targeting of retinal ganglion cell axons in the visual pathway of the brain. *Molecular and*

- Cellular Neuroscience*, 37(4), 719–730. <https://doi.org/10.1016/j.mcn.2007.12.017>
- Plump, A. S., Erskine, L., Sabatier, C., Brose, K., Epstein, C. J., Goodman, C. S., Mason, C. A., & Tessier-Lavigne, M. (2002). Slit1 and Slit2 cooperate to prevent premature midline crossing of retinal axons in the mouse visual system. *Neuron*, 33(2), 219–232. [https://doi.org/10.1016/S0896-6273\(01\)00586-4](https://doi.org/10.1016/S0896-6273(01)00586-4)
- Poulain, F. E., Gaynes, J. A., Hörndli, C. S., Law, M. Y., & Chien, C. B. (2010). Analyzing retinal axon guidance in zebrafish. *Methods in Cell Biology*, 100, 3–26. <https://doi.org/10.1016/B978-0-12-38489-2-5.00001-3>
- Pujic, Z., Giacomantonio, C. E., Unni, D., Rosoff, W. J., & Goodhill, G. J. (2008). Analysis of the growth cone turning assay for studying axon guidance. *Journal of Neuroscience Methods*, 170(2), 220–228. <https://doi.org/10.1016/j.jneumeth.2008.01.014>
- Reczek, C. R., & Chandel, N. S. (2015). ROS-dependent signal transduction. *Current Opinion in Cell Biology*, 33, 8–13. <https://doi.org/10.1016/j.ceb.2014.09.010>
- Robles, E., Filosa, A., & Baier, H. (2013). Precise lamination of retinal axons generates multiple parallel input pathways in the tectum. *Journal of Neuroscience*, 33(11), 5027–5039. <https://doi.org/10.1523/JNEUROSCI.4990-12.2013>
- Ryder, L. S., Dagdas, Y. F., Mentlak, T. A., Kershaw, M. J., Thornton, C. R., Schuster, M., Chen, J., Wang, Z., & Talbot, N. J. (2013). NADPH oxidases regulate septin-mediated cytoskeletal remodeling during plant infection by the rice blast fungus. *Proceedings of the National Academy of Sciences*, 110(8), 3179–3184. <https://doi.org/10.1073/pnas.1217470110>
- Safiulina, V. F., Afzalov, R., Khiroug, L., Cherubini, E., & Giniatullin, R. (2006). Reactive oxygen species mediate the potentiating effects of ATP on GABAergic synaptic transmission in the immature hippocampus. *The Journal of Biological Chemistry*, 281(33), 23464–23470. <https://doi.org/10.1074/jbc.M601627200>
- Sakai, J., Li, J., Subramanian, K. K., Mondal, S., Bajrami, B., Hattori, H., Jia, Y., Dickinson, B. C., Zhong, J., Ye, K., Chang, C. J., Ho, Y.-S., Zhou, J., & Luo, H. R. (2012). Reactive oxygen species-induced actin glutathionylation controls actin dynamics in neutrophils. *Immunity*, 37(6), 1037–1049. <https://doi.org/10.1016/j.immuni.2012.08.017>
- Stein, E., & Tessier-Lavigne, M. (2001). Hierarchical organization of guidance receptors: Silencing of netrin attraction by slit through a Robo/DCC receptor complex. *Science*, 291(5510), 1928–1938. <https://doi.org/10.1126/science.1058445>
- Stuermer, C. A. (1988). Retinotopic organization of the developing retinotectal projection in the zebrafish embryo. *The Journal of Neuroscience*, 8(12), 4513–4530. <https://doi.org/10.1523/JNEUROSCI.08-12-04513.1988>
- Sun, Q. A., Hess, D. T., Wang, B., Miyagi, M., & Stamler, J. S. (2012). Off-target thiol alkylation by the NADPH oxidase inhibitor 3-benzyl-7-(2-benzoxazolyl)thio-1,2,3-triazolo[4,5-d]pyrimidine (VAS2870). *Free Radical Biology and Medicine*, 52(9), 1897–1902. <https://doi.org/10.1016/j.freeradbiomed.2012.02.046>
- Suter, D. M. (2011). Live cell imaging of neuronal growth cone motility and guidance in vitro. *Methods in Molecular Biology*, 769, 65–86. https://doi.org/10.1007/978-1-61779-207-6_6
- Suzukawa, K., Miura, K., Mitsushita, J., Resau, J., Hirose, K., Crystal, R., & Kamata, T. (2000). Nerve growth factor-induced neuronal differentiation requires generation of Rac1-regulated reactive oxygen species. *Journal of Biological Chemistry*, 275(18), 13175–13178. <https://doi.org/10.1074/jbc.275.18.13175>
- Taulet, N., Delorme-Walker, V. D., & DerMardirossian, C. (2012). Reactive oxygen species regulate protrusion efficiency by controlling actin dynamics. *PLoS One*, 7(8), e41342. <https://doi.org/10.1371/journal.pone.0041342>
- Tejada-Simon, M. V., Serrano, F., Villasana, L. E., Kanterewicz, B. I., Wu, G. Y., Quinn, M. T., & Klann, E. (2005). Synaptic localization of a functional NADPH oxidase in the mouse hippocampus. *Molecular and Cellular Neuroscience*, 29(1), 97–106. <https://doi.org/10.1016/j.mcn.2005.01.007>
- Tenfreyhaus, H., Huntgeburth, M., Wingler, K., Schnitker, J., Baumer, A., Vantler, M., Bekhite, M., Wartenberg, M., Sauer, H., & Rosenkranz, S. (2006). Novel Nox inhibitor VAS2870 attenuates PDGF-dependent smooth muscle cell chemotaxis, but not proliferation. *Cardiovascular Research*, 71(2), 331–341. <https://doi.org/10.1016/j.cardiores.2006.01.022>
- Terzi, A., & Suter, D. M. (2020). The role of NADPH oxidases in neuronal development. *Free Radical Biology and Medicine*, 154, 33–47. <https://doi.org/10.1016/j.freeradbiomed.2020.04.027>
- Thompson, H., Barker, D., Camand, O., & Erskine, L. (2006). Slits contribute to the guidance of retinal ganglion cell axons in the mammalian optic tract. *Developmental Biology*, 296(2), 476–484. <https://doi.org/10.1016/j.ydbio.2006.06.017>
- Thompson, H., Camand, O., Barker, D., & Erskine, L. (2006). Slit proteins regulate distinct aspects of retinal ganglion cell axon guidance within dorsal and ventral retina. *Journal of Neuroscience*, 26(31), 8082–8091. <https://doi.org/10.1523/JNEUROSCI.1342-06.2006>
- Wang, K., Zhang, T., Dong, Q., Nice, E. C., Huang, C., & Wei, Y. (2013). Redox homeostasis: The linchpin in stem cell self-renewal and differentiation. *Cell Death & Disease*, 4(3), e537. <https://doi.org/10.1038/cddis.2013.50>
- Wang, Y., Branicky, R., Noë, A., & Hekimi, S. (2018). Superoxide dismutases: Dual roles in controlling ROS damage and regulating ROS signaling. *Journal of Cell Biology*, 217(6), 1915–1928. <https://doi.org/10.1083/jcb.201708007>
- Weaver, C. J., Leung, Y. F., & Suter, D. M. (2016). Expression dynamics of NADPH oxidases during early zebrafish development. *Journal of Comparative Neurology*, 524(10), 2130–2141. <https://doi.org/10.1002/cne.23938>
- Weaver, C. J., Terzi, A., Roeder, H., Gurol, T., Deng, Q., Leung, Y. F., & Suter, D. M. (2018). nox2/cybb deficiency affects zebrafish retinotectal connectivity. *Journal of Neuroscience*, 38(26), 5854–5871. <https://doi.org/10.1523/JNEUROSCI.1483-16.2018>
- Westerfield, M. (2000). *The Zebrafish book*. University of Oregon Press.
- Wilkinson, R. N., Elworthy, S., Ingham, P. W., & van Eeden, F. J. M. (2013). A method for high-throughput PCR-based genotyping of larval zebrafish tail biopsies. *BioTechniques*, 55(6), 314–316. <https://doi.org/10.2144/000114116>
- Wilson, C., Muñoz-Palma, E., Henríquez, D. R., Palmisano, I., Núñez, M. T., Di Giovanni, S., & González-Billault, C. (2016). A feed-forward mechanism involving the NOX complex and RyR-mediated Ca²⁺ release during axonal specification. *Journal of Neuroscience*, 36(43), 11107–11119. <https://doi.org/10.1523/JNEUROSCI.1455-16.2016>
- Wilson, C., Nunez, M. T., & González-Billault, C. (2015). Contribution of NADPH oxidase to the establishment of hippocampal neuronal polarity in culture. *Journal of Cell Science*, 128(16), 2989–2995. <https://doi.org/10.1242/jcs.168567>
- Xiao, T., Staub, W., Robles, E., Gosse, N. J., Cole, G. J., & Baier, H. (2011). Assembly of lamina-specific neuronal connections by slit bound to type IV collagen. *Cell*, 146(1), 164–176. <https://doi.org/10.1016/j.cell.2011.06.016>

- Zhang, C., Gao, J., Zhang, H., Sun, L., & Peng, G. (2012). Robo2-Slit and Dcc-netrin1 coordinate neuron axonal pathfinding within the embryonic axon tracts. *Journal of Neuroscience*, *32*(36), 12589–12602. <https://doi.org/10.1523/JNEUROSCI.6518-11.2012>
- Zhou, F. Q., & Cohan, C. S. (2001). Growth cone collapse through coincident loss of actin bundles and leading edge actin without actin depolymerization. *Journal of Cell Biology*, *153*(5), 1071–1083. <https://doi.org/10.1083/jcb.153.5.1071>
- Zhu, X., Xu, Y., Yu, S., Lu, L. U., Ding, M., Cheng, J., Song, G., Gao, X., Yao, L., Fan, D., Meng, S., Zhang, X., Hu, S., & Tian, Y. (2014). An efficient genotyping method for genome-modified animals and human cells generated with CRISPR/Cas9 system. *Scientific Reports*, *4*, 6420. <https://doi.org/10.1038/srep06420>

SUPPORTING INFORMATION

Additional supporting information may be found online in the Supporting Information section.

How to cite this article: Terzi A, Roeder H, Weaver CJ, Suter DM. Neuronal NADPH oxidase 2 regulates growth cone guidance downstream of slit2/robo2. *Develop Neurobiol.* 2020;00:1–19. <https://doi.org/10.1002/dneu.22791>